

The Tully-Fisher relation of intermediate redshift field and cluster galaxies from Subaru spectroscopy [★]

O. Nakamura^{1†}, A. Aragón-Salamanca¹, B. Milvang-Jensen², N. Arimoto³,
C. Ikuta³, S. P. Bamford¹

¹*School of Physics and Astronomy, University of Nottingham, University Park, Nottingham, NG7 2RD, UK*

²*Max-Planck-Institut für extraterrestrische Physik, Giessenbachstraße, 85748 Garching, Germany*

³*National Astronomical Observatory, 2-21-1 Osawa, Mitaka, Tokyo 181-8588, Japan*

Accepted ???. Received ???; in original form ???

ABSTRACT

We have carried out spectroscopic observations in 4 cluster fields using Subaru’s FO-CAS multi-slit spectrograph and obtained spectra for 103 bright disk field and cluster galaxies at $0.06 \leq z \leq 1.20$. Seventy-seven of these show emission lines, and 33 provide reasonably-secure determinations of the galaxies’ rotation velocity. The rotation velocities, luminosities, colours and emission-line properties of these galaxies are used to study the possible effects of the cluster environment on the star-formation history of the galaxies. Comparing the Tully-Fisher relations of cluster and field galaxies at similar reshifts we find no measurable difference in rest-frame B -band luminosity at a given rotation velocity (the formal difference is 0.18 ± 0.33 mag). The colours of the cluster emission line galaxies are only marginally redder in rest-frame $B - V$ (by 0.06 ± 0.04 mag) than the field galaxies in our sample. Taken at face value, these results seem to indicate that bright star-forming cluster spirals are similar to their field counterparts in their star-formation properties. However, we find that the fraction of disk galaxies with absorption-line spectra (i.e., with no current star formation) is larger in clusters than in the field by a factor of ~ 3 –5. This suggests that the cluster environment has the overall effect of switching off star formation in (at least) some spiral galaxies. To interpret these observational results, we carry out simulations of the possible effects of the cluster environment on the star-formation history of disk galaxies and thus their photometric and spectroscopic properties. This allows us to create mock samples of unperturbed “field” galaxies (with approximately constant star-formation rates) and perturbed “cluster” galaxies with different star-formation histories, including star formation truncation, with or without an associated starburst. We show that, if we select only bright galaxies with current star-formation (i.e., with emission lines strong enough for rotation-curve measurements), the average colours and luminosities of the “cluster” galaxies may not be very different from those of galaxies in the “field” sample, even though their star-formation histories may be significantly different. However, the fraction of emission and absorption-line galaxies would change significantly. We also use these simulations to estimate the size of field and cluster galaxy samples that would allow us to differentiate the different star-formation scenarios considered. Finally, we find that the rest-frame absolute B -band magnitude of the field galaxies in our sample shows an evolution of -1.30 ± 1.04 mag per unit redshift at fixed rotation velocity. This indicates that the average SFR of bright disk galaxies evolves more slowly than the universal star-formation rate as determined from UV, H α , far-infrared and radio studies. This suggests the evolution of the universal SFR density is not dominated by bright star-forming disk galaxies, in agreement with previous studies.

Key words: galaxies: clusters: general – galaxies: evolution – galaxies: kinematics and dynamics – galaxies: spiral

1 INTRODUCTION

Recent studies of distant galaxies have established that the fraction of S0s in rich galaxy clusters drops by a factor 2–3 from the local universe to $z \sim 0.5$, while the fraction of spiral galaxies increases comparatively (Couch et al. 1994; Dressler et al. 1997; van Dokkum et al. 1998; Fasano et al. 2000). Parallel studies have found a number of poststarburst galaxies within clusters (Dressler & Gunn 1983; Couch & Sharples 1987), a suppressed star formation rate for spiral types relative to the field (Balogh et al. 1998), and evidence of an infalling spiral population out to $z \sim 0.4$ (Poggianti et al. 1999; Kodama & Bower 2001). This naturally leads to the scenario that cluster S0s could form from spiral galaxies through interaction with the cluster environment (Jones, Smail & Couch 2000; Kodama & Smail 2001).

Three mechanisms have been suggested for the transformation: galaxy-galaxy interactions, tidal forces, and gas stripping. Galaxy-galaxy interaction is most efficient in group environments, where relative velocities are low (Zabludoff & Mulchaey 1998; Mulchaey & Zabludoff 1998; Ghigna et al. 1998), while tidal forces (Toomre & Toomre 1972; Moore et al. 1996; Mihos, McGaugh, & de Blok 1997) are effective on small spirals. Gas stripping is expected to be an effective process in rich clusters (Abadi, Moore, & Bower 1999; Quilis, Moore, & Bower 2000; Bekki, Couch, & Shioya 2002; Vogt et al. 2004). Although each mechanism is efficient in different circumstances and/or environments, many of the numerical studies of these mechanisms predict a starburst could/should happen during the processes leading to the cessation of star formation required by the spiral-to-S0 transformation.

Until recently, however, there has been no compelling evidence indicating that spiral galaxies falling into dense environments experience a star-burst. Motivated by this Ziegler et al. (2003) investigated three clusters at $z = 0.3$ – 0.5 and used the Tully-Fisher relation (TFR) to compare galaxy luminosities of field and cluster spirals at the same mass, finding no measurable difference. In contrast, Milvang-Jensen et al. (2003) carried out a similar study for the rich cluster MS1054.4–0321 at $z = 0.83$, and found evidence for some brightening in the cluster galaxies relative to the field ones at the same rotation velocity, implying more active star-formation of spiral galaxies in clusters. The situation is thus controversial, but these studies showed that using the TFR as a tool for comparing field and cluster galaxies at intermediate redshift could be successful.

Following Milvang-Jensen et al., we have carried out a study of the TFR in nine additional distant rich clusters. Five have been observed with the VLT using the FORS2 multi-slit spectrograph (Seifert et al. 2000) and the results (including a re-analysis of the MS1054.4–0321 data) have been reported in Bamford et al. (2005A, B05A hereafter), where they have found further evidence for the brightening in the cluster spirals. In this paper, we report on our TFR study for the remaining four clusters observed with the Subaru Telescope using the FOCAS spectrograph (Kashikawa et al. 2002). Since our sample includes field galaxies, we also discuss their evolution following Bamford, Aragón-Salamanca & Milvang-Jensen (2005B, B05B hereafter).

Before comparing the cluster spiral galaxies with the

field ones, one needs to be aware that the comparison could be complicated by strong selection effects. For example, the probability of observing a galaxy in a star-burst phase will be lower if the star-formation occurs over a short time-scale; on the other hand, a star-bursting galaxy will be brighter, and thus more likely to appear in a magnitude limited sample. Similarly, one could think that if our sample contains galaxies in the fading phase after the starburst has ended, the average luminosity of our sample would be lowered, perhaps cancelling the effect of the initial brightening. However, it is unlikely that we will be able to measure rotation curves for galaxies after the cessation of star formation since emission lines would be absent. All these effects will probably affect the average properties of the galaxies in our field and cluster samples, so we have carried out careful modeling for the correct interpretation of the observations.

Throughout the paper, we assume $\Omega_m = 0.3$, $\Omega_\Lambda = 0.7$, and $H_0 = 70 \text{ km s}^{-1} \text{ Mpc}^{-1}$. All magnitudes are in the Vega zero-point system.

2 DATA

2.1 Observations and data reduction

Our sample contains rich clusters, mainly in the northern hemisphere, covering a wide redshift range, similar to B05A. Table 1 lists the clusters observed, together with some of their properties and basic observational parameters. The MS2053.7–0449 cluster was also studied by B05A, so we should be able to test the consistency of the rotation velocity measurements.

Pre-imaging in the R -band was carried out on 2002 June 7 using FOCAS in imaging mode. The field-of-view was 6 arcmin diameter, and the pixel scale was $0.1 \text{ arcsec pixel}^{-1}$. Each field was taken at two different position angles to enable flexible allocation of tilted slits (see below). The exposure times at each position angle were 180s for A2390 and 240s for the other clusters. The seeing was $0.5\text{--}0.6 \text{ arcsec}$. The images at the different position angles were combined, and SExtractor version 2.0 (Bertin & Arnouts 1996) was used to identify the objects. The photometry was calibrated to Thuan & Gunn (1976) r -band (see Sec.2.3).

For multi-object spectroscopy (MOS) targeting, we determined the priority of each galaxy according to how many of the following conditions were met: (i) disk morphology in pre-imaging (must), (ii) bright enough to observe, (iii) inclination $\gtrsim 45^\circ$, (iv) HST images available from the archive, (v) magnitudes and/or the redshift available from literature, and (vi) known to be a cluster member. We designed the masks by allocating slits to galaxies with the highest priorities. The slits were to be placed along the major axis of galaxies to measure rotation velocities. Two masks with complementary position angles were designed for each cluster except MS2053.7–0449 for which we decided to use only one mask. This allowed us to use slit angles $\lesssim 45^\circ$ relative to the spatial direction for most galaxies, avoiding degrading the resolution beyond acceptable limits. A few slits included more than one galaxy by chance. Table 1 gives the details of the masks. In total 108 slits were placed on 116 galaxies in 7 masks, of which 4 galaxies were observed in two masks and 112 were unique. In the following we always refer to the

number of unique galaxies unless stated. The morphological distribution of the selected galaxies is discussed in Sec. 2.5. The procedures followed for target selection, priority allocation and mask design were very similar to those used by B05A.

The spectroscopic observations were carried out on 2002 Aug 10–11 using FOCAS in MOS mode. The 300B grism was used, yielding a dispersion of $1.4 \text{ \AA pixel}^{-1}$. The slit width was 0.6 arcsec along the dispersion axis for all the objects, achieving a spectral resolution $R \simeq 1200$, slightly higher than B05A. The lower limit of the spectral range was set to 4700 \AA by the order blocking filter, and the upper limit was up to 9400 \AA , depending on the geometrical position of each slit on the mask. The seeing, determined from the spectra of ~ 2 stars observed in each mask, was $0.4\text{--}0.7 \text{ arcsec}$, and we binned $\times 2$ along the spatial direction, achieving a final spatial sampling of $0.2 \text{ arcsec pixel}^{-1}$ for untilted slits. Given the differences in redshift, we made shorter exposures for A2390 and longer ones for MS2053.7–0449 to achieve roughly the same depth in every cluster. Table 1 gives the exposure time of each mask.

Bias subtraction, flat fielding, connection of the two CCD detectors, and distortion correction were done using the FOCASRED package, developed by the instrument team. Wavelength calibration and sky-subtraction were carried out with standard IRAF tasks to obtain the 2-dimensional spectra.

2.2 Redshift and cluster membership

The centre of each galaxy on the 2D spectrum was identified by the peak of the continuum component without emission lines. Central spectra were extracted for each galaxies in $0.2\text{--}0.6 \text{ arcsec}$ apertures, and the redshift was measured using emission and/or absorption features. When more than one emission line were well detected, the mean of the redshifts was taken. The emission lines included $[\text{O II}]\lambda 3727$, $\text{H}\delta$, $\text{H}\gamma$, $\text{H}\beta$, $[\text{O III}]\lambda 4959$, $[\text{O III}]\lambda 5007$, $[\text{N II}]\lambda 6548$, $\text{H}\alpha$, $[\text{N II}]\lambda 6583$, $[\text{S II}]\lambda 6716$, and $[\text{S II}]\lambda 6731$. The redshifts of 77 galaxies were measured in this way. When emission features were not seen, absorption features were used instead. We employed a cross-correlation method with a model template spectrum. Redshifts for 27 absorption-line galaxies were measured in this way. We could not determine the redshifts of 8 galaxies because of poor detection of their absorption features or dubious emission line identification. We drop these galaxies from further analysis, and the remaining is 104. The redshift range of the galaxies was $0.06 \leq z \leq 1.20$ with median of $z = 0.42$. When considering only the galaxies in the final TFR sample (see Sec. 2.4), the redshift range was $0.06 \leq z \leq 0.74$, with a median of $z = 0.39$.

The field-of-view of FOCAS was too small to cover the whole of the clusters, so cluster membership was decided on the basis of velocity only, without considering the spatial location of the galaxies. Galaxies with velocities within $\pm 3\sigma$ from the velocity centre of the cluster were classified as cluster members. The fraction of cluster and field galaxies were 48% and 52%, respectively. The numbers for each cluster are summarised in Table 2.

Table 1. Summary of the clusters and spectroscopic observations.

Cluster	R.A. (J2000)	Dec. (J2000)	z	σ (km s ⁻¹)	Mask ID	P.A. (deg)	T_{exp} (s)	Seeing (arcsec)	N_{slit}	N_{gal}	N_{dup}^c
A2390 ^a	21 53 36.8	+17 41 32	0.2282	1294	P1	0°	1200 × 4	0.7	12	14	1
					P2	-45°	1200 × 3	0.5	13	13	
MS1621.5+2640 ^a	16 23 34.5	+26 34 17	0.4271	735	P1	45°	1800 × 4	0.4	15	17	1
					P2	-45°	1800 × 4	0.6	15	16	
MS0015.9+1609 ^a	00 18 33.5	+16 26 03	0.5490	984	P1	0°	1800 × 5	0.5	16	16	2
					P2	90°	1800 × 5	0.5	20	22	
MS2053.7-0449 ^b	20 53 44.6	-04 49 16	0.583	817	P1	0°	1800 × 5	0.4	17	18	

^a Position, z and σ from Girardi & Mezzetti (2001).

^b Position and z from Stocke et al. (1991), σ from Hoekstra et al. (2002).

^c Number of galaxies observed in two masks.

2.3 Absolute B -band magnitudes and inclinations

To supplement the pre-imaging photometry and obtain colour information, we obtained magnitudes for the targeted galaxies from the literature. We also collected WFPC2 images from the archive, as in B05A. The available sources of photometry, other than our own FOCAS pre-imaging, were the following: for A2390, the CNOC survey (Yee et al. 1996) and WFPC2 images ($F555W$, $F702W$, $F814W$); for MS1621.5+2640, CNOC (Ellingson et al. 1997) plus WFPC2 ($F555W$, $F814W$); for MS0015.9+1609, CNOC (Ellingson et al. 1998) plus data from Dressler & Gunn (1992), and WFPC2 ($F555W$, $F814W$); for MS2053.7-0449, WFPC2 images ($F606W$, $F702W$, $F814W$). Note that not all these data were available for all of our targeted galaxies (see below).

The CNOC survey used the Thuan & Gunn photometric system and provides r -band total magnitudes and $g-r$ colours within 6.4 arcsec apertures. Dressler & Gunn (1992) used Schneider, Gunn, & Hoessel (1983) photometric system, and give total g -band magnitudes and $g-r$ and $r-i$ colours within the fitting radius. The WFPC2 images were extracted from the archive with the basic reductions completed. We ran SExtractor for these images and obtained AUTOMAGs, which provide good estimates of total magnitudes within 0.1 mag. This uncertainty in the total magnitude is too small to have any effect on our TFR analysis. The zero-points were calibrated with reference to the latest WFPC2 manual. The available HST photometric bands differed from cluster to cluster and object to object, but at least two bands were always available, so we had some colour information for every galaxy within the WFPC2 field. The redder bands were used to define the aperture centres when deriving colours. The FOCAS pre-imaging was not photometrically-calibrated at the telescope, so that photometry was calibrated using the galaxies that were in common with the CNOC. A constant offset was used to transform SExtractor’s AUTOMAG in the pre-imaging to the total Thuan & Gunn r -band magnitudes from CNOC. The error of this calibration was ~ 0.08 mag, estimated from the $r.m.s.$ of the transformation. Thus, the magnitudes derived from the FOCAS pre-imaging are in the Thuan & Gunn r -band system.

For each galaxy, the magnitude in the band that was closest to the rest-frame Johnson-Morgan B -band was chosen among those available as the starting point to calculate

rest-frame B magnitudes. To obtain a representative colour we used the data from the CNOC, WFPC2, and Dressler & Gunn (1992) (in that order of priority). The Galactic extinction of Schlegel, Finkbeiner, & Davis (1998) was applied to these magnitudes and colours. The magnitude was then converted to the absolute rest-frame B -band magnitude by referring to the galaxy colours and K -corrections of Fukugita, Shimasaku, & Ichikawa (1995). The concordance cosmology (cf. §1) was used to calculate the distance modulus. In many cases we had several colours available from different sources, allowing us to estimate that the error in the rest-frame B -band magnitude associated with using different colours was 0.03 mag on average. Moreover, we estimate that the error associated with using different photometric bands to estimate rest-frame B -band was 0.08 mag on average. This indicates that the values of our rest-frame B magnitudes are quite robust, with uncertainties of the order of 0.1 mag or less.

In a few cases the only available photometry came from the FOCAS pre-imaging. In that case, the rest-frame B magnitude was estimated from the pre-imaging magnitude applying an Sc galaxy K -correction. Nine objects belong to this category, with only four making it to the final TFR study.

The inclination of the disk component was measured using GIM2D (Simard et al. 2002) following B05A. The WFPC2 images were used whenever available, while the pre-imaging was used otherwise. When the WFPC2 images were used, we always selected the band with the highest S/N, yielding the highest confidence. There were 48 galaxies with an inclination $i > 40^\circ$ (i.e., large enough for reliable rotation velocity determination) which had their inclinations measured in both the pre-imaging and the WFPC2 $F814W$ images. For these galaxies, the average ratio of the $(\sin i)^{-1}$ values determined from the pre-imaging and HST data respectively was 1.02 ± 0.01 . Similarly, there were 39 galaxies with $i > 40^\circ$ that had their inclinations determined from $F555W$ and $F814W$. For these, the average $(\sin i)^{-1}$ ratio was 0.98 ± 0.01 . Hence the systematic error in mixing the inclinations obtained from the different WFPC2 bands and the pre-imaging is only $\sim 2\%$, and can be safely ignored. Note that the FOCAS images had very good seeing, and the value of the inclination is dominated by the outer isophotes, making our ground-based data perfectly adequate for inclination determination at these moderate redshifts.

Finally, the internal reddening was corrected as a func-

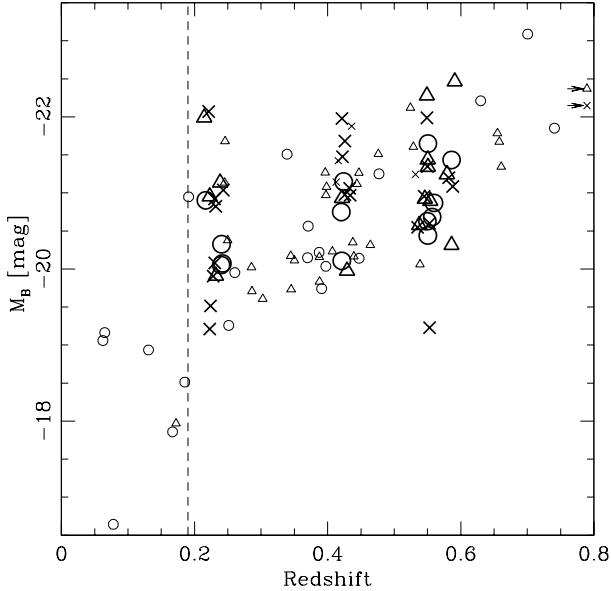


Figure 1. Absolute B -band magnitude vs. redshift for the 104 galaxies with measured redshifts. The different symbols indicate absorption-line galaxies (crosses), emission-line galaxies (triangles), and emission-line galaxies with measured rotation velocity (circles). Small and large symbols denote field and cluster galaxies, respectively. The two marks with arrows are the galaxies at $z = 1.195$ (cross) and 1.041 (triangle). The dashed line at $z = 0.19$ is used to define an unbiased sample for our analysis (see text for details).

tion of inclination following the prescription of Tully & Fouque (1985). The absolute extinction at face-on position was assumed to be 0.27 mag in B following B05A. The derived absolute B -band magnitudes (M_B) are shown in Fig. 1 as a function of redshift.

There were seven galaxies in common with the VLT sample of B05A in the MS2053.7–0449 field. Our B -band magnitudes for these agreed well with those by B05A, with five out of the seven being within 0.1 mag. This ensures the consistency of the derived magnitudes even though we used partly different procedures and photometric sets from B05A in our derivation.

Our sample does not contain enough bright galaxies at the lower end of the redshift range due to the small observed volume. Since this could cause a bias in our analysis, we will only consider galaxies with $z > 0.19$ in our study. In doing so we ensure that our field and cluster samples contain galaxies covering similar luminosity ranges ($-22.5 \lesssim M_B \lesssim -19.5$). The redshift and magnitude ranges studied here are comparable to the ‘matched’ sample of B05A ($z > 0.25$ and $M_B < -19.5$), although we do not reach the redshift of their most distant cluster (MS1054.4–0321 at $z = 0.83$).

2.4 Rotation velocities

In order to be able to measure the rotation velocities of the 77 galaxies with detected emission lines (see Table 2), we first fitted the continuum component and removed it in each spectrum by interpolation. Then every emission line was cut

out to a postage stamp image, and input to the software ELFIT2PY (B05A) together with the inclination and the absolute B -band magnitude to measure the rotation velocity. ELFIT2PY is based on the algorithm of ELFIT2D (Simard & Pritchett 1998, 1999), and calculates the best fitting the rotation velocity and scale-length of the emission assuming an intrinsic rotation curve and an exponential light distribution. The software takes into account the instrumental resolution and the seeing, as well as the slit width (optical beam smearing). The output rotation velocity has to be corrected for inclination. The inclination is also necessary as an input to calculate the light distribution through the slit. The absolute B -band magnitude is taken into account in the fitting process since we assumed the universal rotation curve of Persic & Salucci (1991). The output rotation velocity would change, on average, by $\sim 10 \text{ km s}^{-1}$ if we adopted a flat rotation curve, the exact value depending on the luminosity/mass of the galaxy (cf. B05A). Such small change would not affect the conclusions of this study. The spatial centre was determined from the centroid of the continuum, while we allowed ± 1 pixel flexibility in the velocity centre ($\sim 76 \text{ km s}^{-1}$ at 5500 \AA and $z = 0$) to let ELFIT2PY account for possible errors in redshift and wavelength calibration. In fact, of the objects used in the final TFR (see below) 85% had offsets of 0.2 pixels or less.

As part of the rotation velocity determination we carried out a quality-control process to ensure that only reliable measurements were used in the analysis. Our process is similar to the one used by B05A, so we will only describe here briefly the main quality-control steps. First, we did not attempt to measure the rotation velocities when the emission was nuclear (i.e., spatially-unresolved) or when the mean S/N was below a given threshold. Second, when measurement yielded a rotation velocity smaller than its estimated 1σ error, we rejected the measurement as unreliable. Third, the fits were visually inspected and those clearly wrong were also rejected. The main causes for rejection included: not reaching the flat rotation or the turn-over point (cf. Verheijen 2001), clear non-exponential distribution of the emission, strong asymmetry, and a deep stellar absorption close to the emission. In a few cases the slits appeared to have been cut in the wrong direction, so these galaxies were also rejected. Note that our treatment of the turn-over point is different from that of B05A, and we will discuss this issue in Sec. 4. After this process, only 33 galaxies (43%) with detected emission lines yielded secure rotation velocities that we can reliably use in the final TFR analysis. For reference, we attempted to fit 63 galaxies using ELFIT2PY, of which 15 were rejected due to clear velocity under-estimates by ELFIT2PY or no sign of turn-over, 9 for low quality fits, 2 for lack of rotation structure, and 4 for problems not directly related to the rotation velocity measurement.

When more than one emission line were securely measured for a galaxy, we used the velocity measured using the line with the highest S/N , while B05A took the error-weighted mean value. The number of emission lines measured per galaxy was 2.5 on average for the 33 galaxies, and 25 of these had more than one emission line. The ratio of the rotation velocities determined with the two highest S/N lines has a mean of 0.97 and a standard deviation of 0.11. Hence the rotation velocities of the different emission lines were consistent with each other typically within 11%.

In Fig. 2 we show the observed rotation curves of the 33 galaxies in the final sample, together with the fitted models, in order to give a visual impression of the quality of the data and the fits. We note that a few galaxies may have irregular kinematics (e.g. C0016.P1 11_A). Examples of objects rejected by our quality-control procedure are shown in Fig. 3. The rejected objects were not used in our analysis.

The measured rotation velocities were corrected for inclination multiplying them by $(\sin i)^{-1}$. The uncertainties in the final values were estimated taking into account the errors in the inclinations from GIM2D, and the errors in the rotation velocities from ELFIT2PY. Table 2 provides some statistics for the spectroscopic data.

The internal consistency of the rotation velocities was checked using four galaxies observed in two different masks. Three of them showed emission lines. After the quality-control process, two galaxies were left with only one acceptable spectrum due to slit angles being more than 60 degrees and/or having rotation curves of insufficient quality from the other spectrum. Thus, for only one galaxy we measured two good-quality rotation velocities from two independent spectra (M1621.P1 12_A and M1621.P2 10_A). These rotation velocities were 163_{-8}^{+12} and 186_{-14}^{+12} (km s⁻¹) respectively (before inclination correction). These measurements were thus consistent ($\sim 1.3\sigma$ discrepancy), and the second value was chosen for the final sample due to marginally better S/N in the spectrum.

The excellent seeing of the Subaru observations and the relatively high spectral resolution of the FOCAS data allowed us to test the effect of the seeing and the instrumental resolution in the measurement of the rotation velocities. This is important when comparing with the VLT results (cf. B05A), obtained in poorer seeing and with slightly lower spectral resolution. The spectra of the surviving 33 galaxies were convolved with Gaussians to simulate a ~ 1.0 arcsec seeing and a spectral resolution $R \sim 950$. These values roughly correspond to the VLT data of B05A. The rotation velocities were then measured in the same way. The ratio of the rotation velocity determined from the convolved spectrum to the original one was 1.02 ± 0.03 , and no systematic trend was found as function of fitted emission scale-length. Hence we should be able to compare our data with that of B05A without any correction. We note that this applies only to the galaxies with secure rotation velocities in our sample, and does not necessarily mean that the method we have used to measure rotation velocities is not affected by the seeing conditions.

Among the seven galaxies that we have in common with the VLT data of B05A (Sec. 2.3), three galaxies yielded secure rotation velocities. Unfortunately, only one of these, M2053.P1 07_A in Fig. 2, was measured securely by B05A. Our velocity estimate for this galaxy was 182_{-17}^{+19} km s⁻¹ before inclination correction, while B05A obtained 154_{-10}^{+11} km s⁻¹. Although this is our only direct comparison, the results are consistent with each other within 1.4σ . The fully-corrected magnitudes, rotation velocities, and colours of our sample are summarized in Table 3.

2.5 Morphologies

The morphology of the galaxies was double-checked on the HST images after the observations were completed. Al-

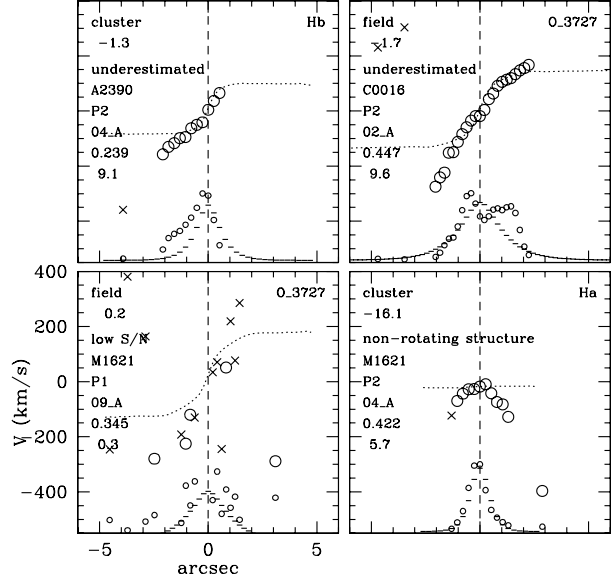


Figure 3. Examples of rotation velocity measurements which have been identified as insecure and thus rejected. The reasons are written at the left-upper part of each panel. The symbols and lines are the same as in Fig. 2.

Table 4. Visual Morphology of 62 galaxies for which HST images are available.

	Cluster		Field		Total
	N_{em}	N_{abs}	N_{em}	N_{abs}	
Total	15	13	34	0	62
S0	$\lesssim 1$	$\lesssim 6$	$\lesssim 2$	0	$\lesssim 9$

though the FOCAS imaging allowed us to reliably select disk galaxies, it didn't have enough resolution to separate S0s from spirals. Among the 104 galaxies targeted, 62 had been imaged with HST. Some statistics of our visual inspection are given in Table 4. As we targeted disk galaxies (see Sec. 2.1), our sample includes no elliptical galaxies except for one that happened to be on the slit of another target and was identified as a cluster member of A2390. Sometimes it was difficult to distinguish S0s from spirals even with the HST-images. Although we did not find any clear S0 galaxies, we did find some galaxies for which the classification was dubious. For that reason, Table 4 gives an upper limit to the number of S0s in our sample. By design, most galaxies in our sample turned out to be spirals. We estimate that at most $\sim 50\%$ of the galaxies with absorption-line spectra were S0s. We will come back to this issue later. We note that all the galaxies in the final TFR sample (i.e., with secure rotation velocities) that had HST images had clear spiral morphologies, as expected. Postage stamps of the HST/FOCAS images of the galaxies in the final sample are presented in Fig. 4.

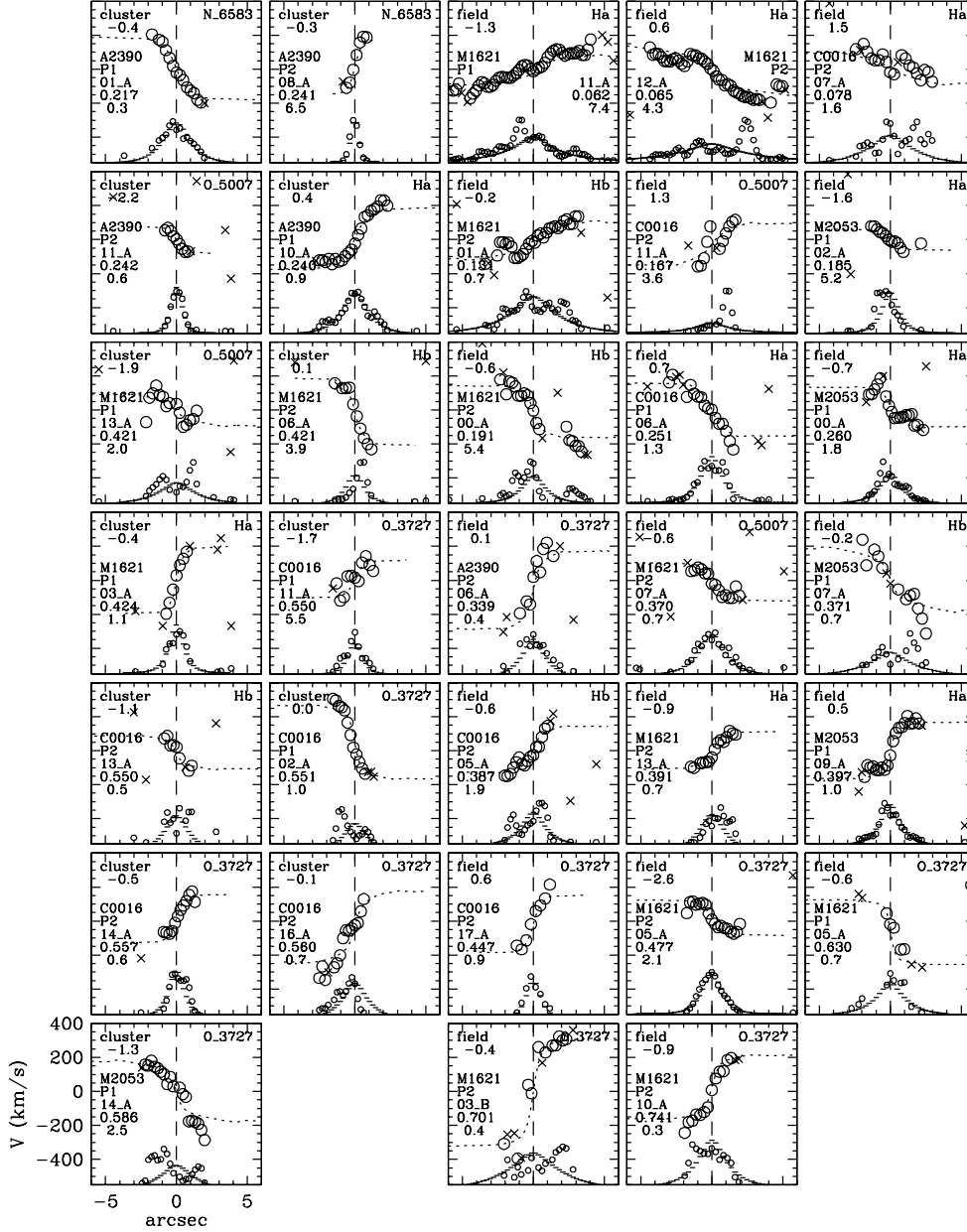
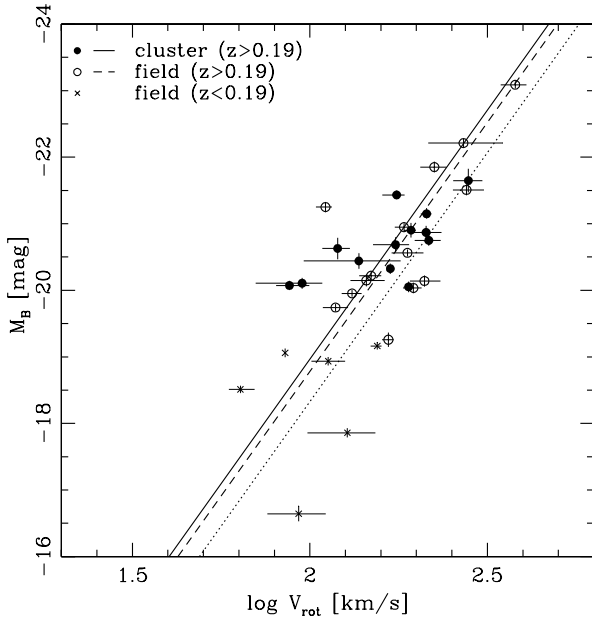


Figure 2. The observed rotation curves of the 33 galaxies that survive our quality-control process and are used in the final TFR analysis. The cluster and field galaxies are displayed in the first two and the last three columns, respectively, in redshift order. The velocities are “observed”, as opposed to “intrinsic”, i.e., not corrected for inclination, non-zero slit width, seeing effects, etc. The vertical dash line shows the spatial centre. The large circles denote the velocity centre determined from Gaussian fits to each spatial column with the peak higher than 2 times the background RMS and the FWHM between 0.7 and 1.4 the resolution. The crosses are the same as the circles but with the peak as low as 0.7 times the background RMS and the FWHM between 0.5 and 2.0. Dotted lines show the ELFIT2PY fitted model when the peak of the Gaussian is above 0.01 times the background RMS. The zero-point of the velocity in each panel is set to the adopted redshift for the object. The small circles and horizontal ticks at the bottom of each panel show the flux distribution of the spectrum and model fit, respectively. The Flux is derived by integrating under the fitted Gaussians. One pixel corresponds to $0.2(\cos\theta)^{-1}$ arcsec where θ is the slit tilt angle. The width of the box is 12.2 arcsec. Labels at the top-left of each panel indicate whether the galaxies belong to the clusters or the field. The numbers right below these labels indicate the residuals, in M_B , from the local TFR (cf. Fig. 6; see Sec. 3.1). The cluster name, mask ID, slit ID, redshift, and χ^2 per fitting element of the galaxies are indicated on the middle-left of each panel. The emission line ID is shown on the top-right corner.

Table 2. Summary of the emission line measurements.

Cluster	Observed			Emission-detected		V_{rot} -measured	
	N_c^a	N_f^b	N_u^c	N_c	N_f	N_c	N_f
A2390	16	8	2	8	6	4	1
MS1621.5+2640	11	18	3	5	17	3	10
MS0015.9+1609	17	16	3	11	15	5	5
MS2053.7-0449	6	12	0	4	11	1	4
Sub-total	50	54	8	28	49	13	20
Total		112			77		33

^a Number of galaxies in clusters.^b Number of galaxies in field.^c Number of galaxies with unknown z .**Figure 5.** The TFR of the 33 galaxies for which reliable rotation velocities were measured. Filled and open circles are the cluster and field galaxies at $z > 0.19$. Field galaxies at $z < 0.19$ (crosses) are kept separated because of possible sampling bias (see Sec. 2.3). The dotted line shows the local TFR of PT92. The solid and the dashed lines show the linear fits to the cluster and the field galaxies at $z > 0.19$ with the slope fixed to that of PT92.

3 RESULTS

The primary purpose of this study is to see whether spiral galaxies in clusters have higher star formation activity than those in the field. In the following, we focus on three different aspects to investigate it: magnitude as function of rotation velocity (i.e., TFR), colour, and fraction of spiral galaxies with absorption-line spectra (i.e., no current star formation).

3.1 Tully-Fisher relation

The TFR of our sample is shown in Fig. 5. There are 6 field galaxies at $z < 0.19$. Although the number is small,

they are consistent with the local TFR of Pierce & Tully (1992; PT92 hereafter; $M_B = -7.48 \log V_{rot} - 3.10 - 0.27^1$). This suggests that our low redshift data is consistent with the results of PT92. The galaxies at $z > 0.19$ tend to be brighter than the local TFR of PT92 when compared at the same rotation velocity. This suggests a possible luminosity evolution at higher redshifts. More on this later.

No clear difference is apparent between the cluster and the field galaxies at $z > 0.19$. Using a simple χ^2 minimization method with internal errors taken into account (cf. B05B), we fitted linear regression lines with the same slope as the local TFR of PT92 to the field and cluster galaxies. We find that the cluster and the field galaxies are 0.64 ± 0.24 and 0.46 ± 0.23 mag brighter, respectively, than the local spirals in PT92. The cluster galaxies appear to be 0.18 mag brighter than the field galaxies, but the difference has no statistical significance.

An obvious problem with the above analysis is that our TFR has been derived for galaxies at different redshifts. If there is luminosity evolution with redshift, it should be taken into account. To assess this issue, in Fig. 6 we plot the residuals (in magnitude) of our TFR from the local one of PT92 as function of redshift. There is a trend suggesting positive luminosity evolution with redshift. A linear fit to the field galaxies at $z > 0.19$ gives

$$\Delta M_B = (-1.30 \pm 1.04) z + 0.09 \pm 0.46. \quad (1)$$

The median redshift of the sample used is $z = 0.39$. The fitted line has $\Delta M_B \sim 0$ at $z = 0$, consistent with the local TFR of PT92. The six field galaxies at $z < 0.19$ are also consistent with the fit. Even taking into account the possible luminosity evolution with redshift, Fig. 6 also suggests that there is no obvious difference in the behaviour of the cluster galaxies from that of the field galaxies. The intrinsic standard deviations around the TFR linear fit, after the luminosity evolution with redshift is taken off, are 0.73 mag and 0.78 mag for the cluster and the field galaxies.

¹ The intercept of the TFR in PT92 may be 0.45 ± 0.12 mag brighter if the difference between H_0 that was derived from the sample of PT92 (Pierce 1994, $86 \text{ km s}^{-1} \text{ Mpc}^{-1}$) and the one used in this paper is taken into account (B05B). Our conclusions are not affected by this issue.

Table 3. The data for the 104 galaxies in our sample with measured redshift. The galaxies are sorted by redshift first for the cluster members and then for the field galaxies. The columns are: (1) cluster, mask and slit IDs; (2) R.A. and (3) Dec.; (4) redshift; (5) cluster (C) or field (F) membership flag; (6) sample status (‘TFR’≡in the final TFR; ‘em’≡emission-line galaxy without secure rotation velocity; ‘abs’≡absorption-line galaxy); (7) inclination ($90^\circ \equiv$ edge-on); (8) absolute rest-frame B -band magnitude, (9) rotation velocity, and (10) rest-frame $B - V$ colour.

Cluster/Mask/Slit	R.A. [J2000]	Dec. [J2000]	z	Mem.	TFR	i [deg]	M_B [mag]	$\log V_{\text{rot}}$ [km s $^{-1}$]	$B - V$ [mag]
A2390 P2 00_A	21 53 45.6	+17 41 48	0.2147	C	em.	68	-21.99 ± 0.06	...	0.59
A2390 P1 01_A	21 53 37.6	+17 44 10	0.2168	C	TFR	77	-20.90 ± 0.11	$2.29^{+0.01}_{-0.02}$	0.81
A2390 P1 00_A	21 53 42.9	+17 40 07	0.2211	C	abs.	39	-22.07 ± 0.05	...	0.57
A2390 P2 03_A	21 53 42.8	+17 41 53	0.2230	C	em.	71	-20.95 ± 0.09	...	0.82
A2390 P1 08_A	21 53 31.6	+17 39 31	0.2230	C	abs.	69	-19.21 ± 0.21	...	0.77
A2390 P2 10_A	21 53 28.9	+17 40 06	0.2240	C	abs.	73	-19.51 ± 0.21	...	0.71
A2390 P1 03_A	21 53 34.9	+17 41 01	0.2280	C	abs.	58	-19.90 ± 0.05	...	0.33
A2390 P2 05_A	21 53 47.0	+17 40 47	0.2301	C	abs.	78	-20.92 ± 0.09	...	0.81
A2390 P2 09_A	21 53 30.0	+17 42 50	0.2304	C	abs.	82	-20.08 ± 0.08	...	0.60
A2390 P1 06_B	21 53 35.2	+17 41 51	0.2318	C	abs.	55	-20.82 ± 0.05	...	0.86
A2390 P1 09_A	21 53 33.4	+17 42 24	0.2322	C	em.	68	-19.91 ± 0.05	...	0.35
A2390 P2 04_A	21 53 27.7	+17 43 13	0.2385	C	em.	35	-21.13 ± 0.07	...	0.29
A2390 P1 10_A	21 53 38.1	+17 43 51	0.2401	C	TFR	78	-20.05 ± 0.08	$2.28^{+0.01}_{-0.01}$...
A2390 P2 08_A	21 53 38.0	+17 43 47	0.2406	C	TFR	79	-20.33 ± 0.08	$2.23^{+0.01}_{-0.01}$	0.66
A2390 P2 11_A	21 53 24.8	+17 42 56	0.2420	C	TFR	71	-20.07 ± 0.07	$1.94^{+0.06}_{-0.04}$	0.50
A2390 P2 02_A	21 53 41.8	+17 42 15	0.2433	C	abs.	65	-21.04 ± 0.10	...	0.81
M1621 P2 06_A	16 23 38.0	+26 35 39	0.4205	C	TFR	67	-20.75 ± 0.08	$2.33^{+0.03}_{-0.04}$	0.56
M1621 P1 13_A	16 23 34.8	+26 30 45	0.4213	C	TFR	81	-20.11 ± 0.08	$1.98^{+0.06}_{-0.13}$...
M1621 P1 00_A	16 23 38.9	+26 35 21	0.4216	C	abs.	69	-21.98 ± 0.06	...	0.88
M1621 P2 04_A	16 23 39.1	+26 36 14	0.4217	C	em.	33	-20.93 ± 0.09	...	0.40
M1621 P1 02_A	16 23 37.6	+26 33 01	0.4224	C	abs.	79	-21.48 ± 0.07	...	0.93
M1621 P1 03_A	16 23 42.3	+26 30 55	0.4240	C	TFR	67	-21.15 ± 0.07	$2.33^{+0.01}_{-0.02}$	0.79
M1621 P2 02_A	16 23 42.5	+26 33 44	0.4260	C	abs.	77	-21.68 ± 0.07	...	0.96
M1621 P2 14_A	16 23 36.5	+26 35 01	0.4260	C	abs.	73	-20.98 ± 0.08	...	0.84
M1621 P2 11_A	16 23 41.5	+26 35 36	0.4292	C	em.	65	-19.97 ± 0.08
M1621 P1 14_A	16 23 38.3	+26 34 28	0.4330	C	abs.	4	-21.06 ± 0.06	...	0.90
M1621 P1 04_A	16 23 38.0	+26 36 10	0.4340	C	abs.	58	-20.97 ± 0.07	...	0.65
C0016 P2 10_A	00 18 27.4	+16 23 03	0.5350	C	abs.	54	-20.55 ± 0.10
C0016 P2 12_A	00 18 40.1	+16 25 07	0.5377	C	em.	55	-20.58 ± 0.12	...	0.77
C0016 P1 13_A	00 18 25.6	+16 24 39	0.5450	C	abs.	81	-20.95 ± 0.11	...	0.96
C0016 P2 15_A	00 18 31.9	+16 24 41	0.5461	C	em.	79	-20.92 ± 0.05	...	0.50
C0016 P2 01_A	00 18 38.9	+16 25 06	0.5490	C	abs.	66	-21.99 ± 0.08	...	0.96
C0016 P2 00_A	00 18 30.9	+16 25 41	0.5492	C	em.	64	-22.28 ± 0.08	...	0.59
C0016 P1 11_A	00 18 29.6	+16 26 36	0.5499	C	TFR	67	-20.63 ± 0.16	$2.08^{+0.03}_{-0.04}$	0.40
C0016 P2 06_C	00 18 22.8	+16 26 05	0.5500	C	abs.	85	-21.35 ± 0.09	...	0.82
C0016 P2 13_A	00 18 29.2	+16 23 11	0.5505	C	TFR	60	-20.44 ± 0.11	$2.14^{+0.12}_{-0.16}$	0.55
C0016 P1 04_A	00 18 23.5	+16 25 09	0.5505	C	em.	57	-21.44 ± 0.13	...	0.71
C0016 P1 05_A	00 18 31.1	+16 22 04	0.5506	C	em.	61	-21.34 ± 0.10	...	0.69
C0016 P1 02_A	00 18 17.8	+16 23 23	0.5507	C	TFR	50	-21.65 ± 0.18	$2.45^{+0.04}_{-0.04}$	0.82
C0016 P2 06_B	00 18 23.0	+16 26 05	0.5530	C	abs.	67	-19.23 ± 0.07	...	0.70
C0016 P2 08_A	00 18 36.5	+16 25 15	0.5530	C	abs.	29	-20.60 ± 0.10	...	0.40
C0016 P2 09_A	00 18 26.2	+16 25 08	0.5542	C	em.	47	-20.89 ± 0.09	...	0.90
C0016 P2 14_A	00 18 35.6	+16 26 49	0.5572	C	TFR	54	-20.68 ± 0.11	$2.24^{+0.04}_{-0.06}$	0.55
C0016 P2 16_A	00 18 34.0	+16 27 00	0.5600	C	TFR	81	-20.87 ± 0.10	$2.33^{+0.04}_{-0.05}$	0.50
M2053 P1 06_A	20 56 20.2	-04 36 42	0.5793	C	em.	73	-21.24 ± 0.05	...	0.73
M2053 P1 16_A	20 56 20.3	-04 38 21	0.5820	C	abs.	85	-21.20 ± 0.21	...	0.71
M2053 P1 13_A	20 56 27.8	-04 34 48	0.5863	C	em.	55	-20.31 ± 0.05	...	0.84
M2053 P1 14_A	20 56 22.1	-04 39 15	0.5863	C	TFR	84	-21.43 ± 0.06	$2.24^{+0.02}_{-0.04}$	0.64
M2053 P1 11_A	20 56 18.5	-04 37 20	0.5880	C	abs.	50	-21.09 ± 0.05	...	0.86
M2053 P1 04_A	20 56 19.5	-04 38 05	0.5909	C	em.	75	-22.47 ± 0.21	...	0.67

ies, respectively. Hence, there is also little difference in the scatter of the TFR of cluster and field galaxies. For our sample, this scatter is about twice that of the local galaxies in PT92. This is probably due to the fact that local TFR stud-

ies concentrate on samples of nice, regular spirals, while the high-redshift samples are, perforce, less clean.

In Fig. 7 we show the cumulative distribution of our TFR residuals from the local relation of PT92. We exclude the galaxies at $z < 0.19$ to avoid possible biases (although

Table 3. Continued.

Cluster/Mask/Slit	R.A. [J2000]	Dec. [J2000]	z	Mem.	TFR	i [deg]	M_B [mag]	$\log V_{\text{rot}}$ [km s ⁻¹]	$B - V$ [mag]
M1621 P1 11_A	16 23 39.7	+26 31 07	0.0624	F	TFR	71	-19.06 ± 0.07	1.93 ^{+0.00} _{-0.00}	0.46
M1621 P2 12_A	16 23 24.0	+26 34 14	0.0650	F	TFR	69	-19.16 ± 0.05	2.19 ^{+0.01} _{-0.02}	0.71
C0016 P2 07_A	00 18 22.1	+16 23 45	0.0781	F	TFR	83	-16.64 ± 0.11	1.97 ^{+0.08} _{-0.09}	0.42
M1621 P2 01_A	16 23 33.9	+26 30 55	0.1308	F	TFR	77	-18.94 ± 0.06	2.05 ^{+0.05} _{-0.05}	0.67
C0016 P2 11_A	00 18 20.1	+16 26 00	0.1670	F	TFR	77	-17.86 ± 0.07	2.11 ^{+0.08} _{-0.11}	0.46
M1621 P1 10_A	16 23 34.8	+26 35 45	0.1721	F	em.	71	-17.97 ± 0.05	...	0.34
M2053 P1 02_A	20 56 22.3	-04 39 58	0.1854	F	TFR	73	-18.51 ± 0.05	1.80 ^{+0.04} _{-0.03}	0.48
M1621 P2 00_A	16 23 46.2	+26 31 55	0.1910	F	TFR	55	-20.95 ± 0.05	2.26 ^{+0.02} _{-0.03}	0.50
A2390 P1 11_A	21 53 33.9	+17 43 23	0.2454	F	em.	77	-21.13 ± 0.10	...	0.43
A2390 P2 01_A	21 53 31.4	+17 41 34	0.2459	F	em.	63	-21.68 ± 0.05	...	0.59
A2390 P1 02_A	21 53 38.2	+17 38 44	0.2500	F	em.	85	-20.38 ± 0.08	...	0.34
C0016 P1 06_A	00 18 39.4	+16 24 18	0.2514	F	TFR	70	-19.26 ± 0.11	2.22 ^{+0.01} _{-0.02}	0.55
M2053 P1 00_A	20 56 27.4	-04 35 27	0.2605	F	TFR	63	-19.95 ± 0.05	2.12 ^{+0.03} _{-0.03}	0.50
C0016 P1 00_A	00 18 27.0	+16 26 58	0.2857	F	em.	58	-20.02 ± 0.17	...	0.82
C0016 P1 12_A	00 18 31.4	+16 25 59	0.2862	F	em.	77	-19.71 ± 0.11	...	0.53
C0016 P1 03_A	00 18 32.1	+16 25 21	0.3025	F	em.	0	-19.61 ± 0.06	...	0.50
A2390 P2 06_A	21 53 32.8	+17 41 20	0.3390	F	TFR	73	-21.51 ± 0.08	2.44 ^{+0.05} _{-0.04}	0.82
M2053 P1 05_A	20 56 20.2	-04 40 16	0.3447	F	em.	73	-20.17 ± 0.05	...	0.78
M1621 P1 09_A	16 23 36.0	+26 34 17	0.3451	F	em.	82	-19.73 ± 0.06	...	0.79
C0016 P2 19_A	00 18 18.2	+16 23 58	0.3501	F	em.	65	-20.11 ± 0.09	...	0.43
M1621 P2 07_A	16 23 40.1	+26 34 04	0.3698	F	TFR	78	-20.15 ± 0.09	2.16 ^{+0.05} _{-0.04}	0.73
M2053 P1 07_A	20 56 19.6	-04 38 47	0.3708	F	TFR	75	-20.56 ± 0.05	2.27 ^{+0.04} _{-0.05}	0.65
C0016 P2 05_A	00 18 21.0	+16 26 13	0.3872	F	TFR	67	-20.22 ± 0.07	2.17 ^{+0.03} _{-0.03}	0.37
C0016 P2 04_A	00 18 17.2	+16 25 34	0.3877	F	em.	43	-20.16 ± 0.08	...	0.54
C0016 P1 14_A	00 18 15.8	+16 23 42	0.3878	F	em.	28	-19.83 ± 0.11	...	0.27
M1621 P2 13_A	16 23 33.7	+26 35 45	0.3911	F	TFR	84	-19.74 ± 0.06	2.07 ^{+0.04} _{-0.04}	0.46
A2390 P1 07_A	21 53 32.5	+17 42 48	0.3964	F	em.	63	-21.27 ± 0.07	...	0.70
M2053 P1 09_A	20 56 32.5	-04 36 27	0.3973	F	TFR	58	-20.03 ± 0.08	2.29 ^{+0.02} _{-0.03}	...
C0016 P2 18_A	00 18 37.8	+16 24 55	0.3974	F	em.	14	-20.97 ± 0.07	...	0.56
M2053 P1 01_A	20 56 14.7	-04 35 45	0.3983	F	em.	44	-21.08 ± 0.05	...	0.40
M1621 P2 03_A	16 23 41.2	+26 32 02	0.4071	F	em.	76	-20.23 ± 0.06	...	0.80
M1621 P1 06_A	16 23 39.0	+26 33 08	0.4130	F	abs.	79	-21.14 ± 0.08	...	0.66
A2390 P2 07_A	21 53 44.7	+17 40 47	0.4160	F	abs.	69	-21.42 ± 0.08	...	0.56
A2390 P1 04_B	21 53 41.9	+17 40 27	0.4360	F	abs.	52	-21.88 ± 0.07	...	0.50
M1621 P2 08_A	16 23 44.2	+26 33 42	0.4378	F	em.	68	-20.35 ± 0.09	...	0.52
M1621 P1 08_B	16 23 33.1	+26 33 40	0.4395	F	em.	62	-20.17 ± 0.08
M2053 P1 03_A	20 56 25.2	-04 35 59	0.4440	F	em.	37	-21.12 ± 0.20	...	0.57
C0016 P2 02_A	00 18 15.6	+16 25 04	0.4471	F	em.	72	-21.26 ± 0.07	...	0.41
C0016 P2 17_A	00 18 19.2	+16 25 43	0.4472	F	TFR	54	-20.14 ± 0.08	2.32 ^{+0.05} _{-0.04}	0.37
M2053 P1 10_A	20 56 24.9	-04 37 37	0.4642	F	em.	42	-20.32 ± 0.14	...	0.53
M1621 P1 01_A	16 23 42.6	+26 31 14	0.4762	F	em.	46	-21.51 ± 0.07	...	0.56
M1621 P2 05_A	16 23 39.4	+26 30 58	0.4772	F	TFR	70	-21.25 ± 0.08	2.04 ^{+0.02} _{-0.03}	0.38
A2390 P1 06_A	21 53 35.3	+17 41 55	0.5244	F	em.	35	-22.12 ± 0.08	...	0.53
M2053 P1 08_A	20 56 18.7	-04 34 30	0.5289	F	em.	85	-21.61 ± 0.05	...	0.83
C0016 P1 01_A	00 18 18.5	+16 24 01	0.5320	F	abs.	50	-21.24 ± 0.11	...	0.96
M2053 P1 15_A	20 56 28.8	-04 39 40	0.5387	F	em.	51	-20.06 ± 0.06	...	0.83
M1621 P1 05_A	16 23 47.5	+26 35 01	0.6300	F	TFR	44	-22.21 ± 0.07	2.43 ^{+0.11} _{-0.10}	0.66
C0016 P1 09_A	00 18 32.8	+16 22 18	0.6550	F	em.	72	-21.79 ± 0.08	...	0.82
C0016 P1 07_A	00 18 32.8	+16 26 09	0.6578	F	em.	74	-21.67 ± 0.13	...	0.46
M1621 P2 09_A	16 23 31.9	+26 36 30	0.6608	F	em.	20	-21.34 ± 0.08
M1621 P2 03_B	16 23 41.2	+26 32 00	0.7006	F	TFR	57	-23.09 ± 0.05	2.58 ^{+0.03} _{-0.04}	0.66
M1621 P2 10_A	16 23 32.8	+26 32 00	0.7407	F	TFR	56	-21.85 ± 0.08	2.35 ^{+0.03} _{-0.04}	...
M2053 P1 12_A	20 56 23.7	-04 37 04	1.0410	F	em.	72	-22.37 ± 0.35	...	0.53
M2053 P1 13_B	20 56 27.8	-04 34 49	1.1950	F	abs.	9	-22.15 ± 0.09

the results would not change if we included them). The distribution of the cluster galaxies resembles that of the field galaxies. The same conclusion is observed after the measured luminosity evolution with redshift is taken off by Eq. (1). A Kolmogorov-Smirnov test indicates that the significance of

the difference between the cluster and the field galaxies is 56% for the raw values, reducing to 21% after the evolution is subtracted.

One might suspect that in the process of rotation velocity determination and quality-control (Sec. 2.4) we may

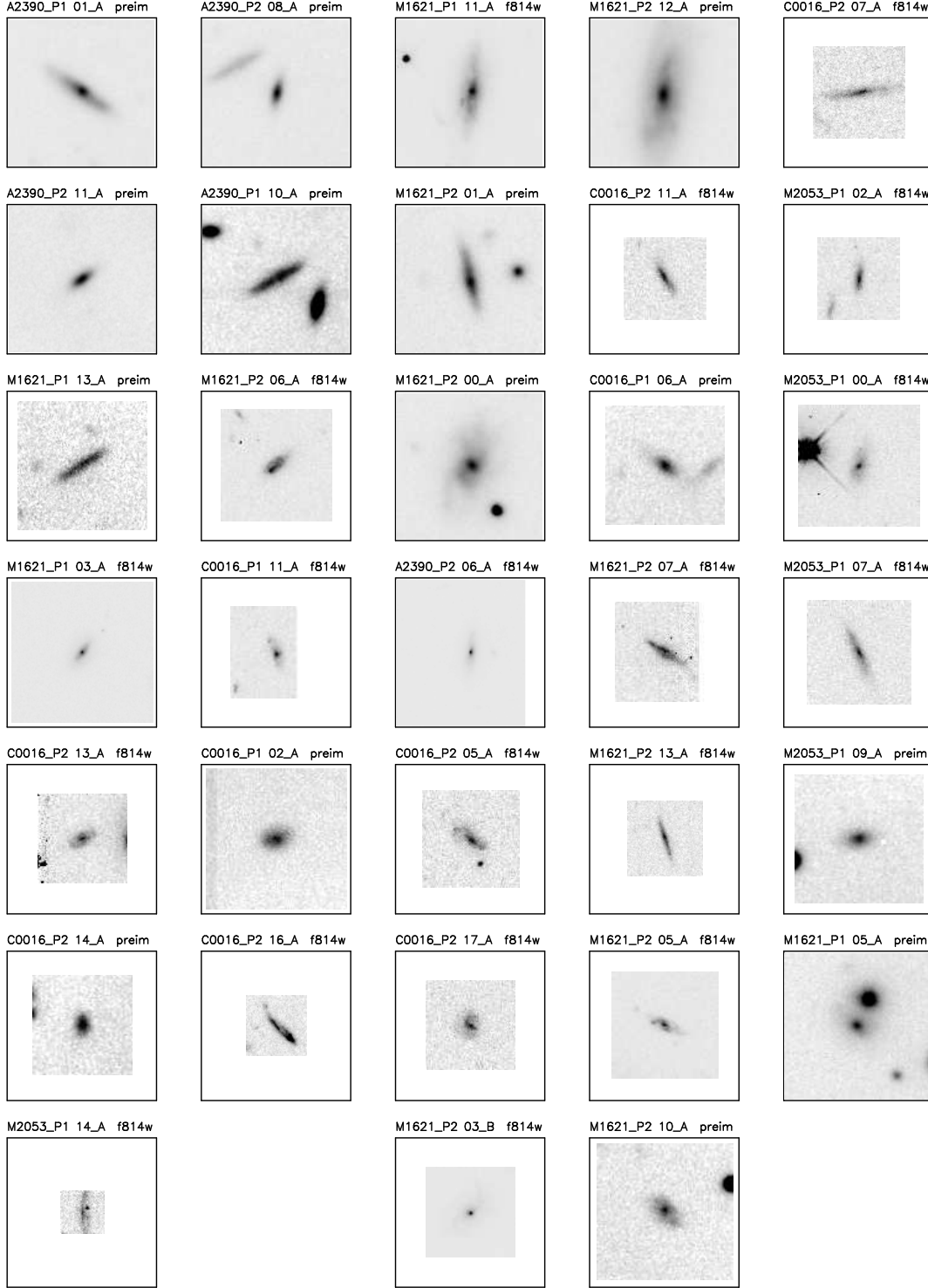


Figure 4. HST/FOCAS images of the galaxies in our final TFR sample. We show HST images (labeled with band IDs) when available, and FOCAS images (marked ‘preim’) otherwise. The size of the box is $12''.2 \times 12''.2$, the same as the spatial dimension used in Fig. 2. The panels are arranged as in Fig. 2.

have missed a number of cluster galaxies that are undergoing a strong star-formation episode with irregular kinematics. A simple test for this possible effect is to compare the fraction of emission-line galaxies which have secure rotation velocities for the cluster and the field samples. According to

Table 2, the respective fractions for cluster and field galaxies are $46 \pm 13\%$ and $41 \pm 9\%$, using Poissonian errors (see also Ziegler et al. 2003). Since these fractions are very similar, there is no clear indication that such a selection bias is introduced by our quality control. In conclusion, there is no

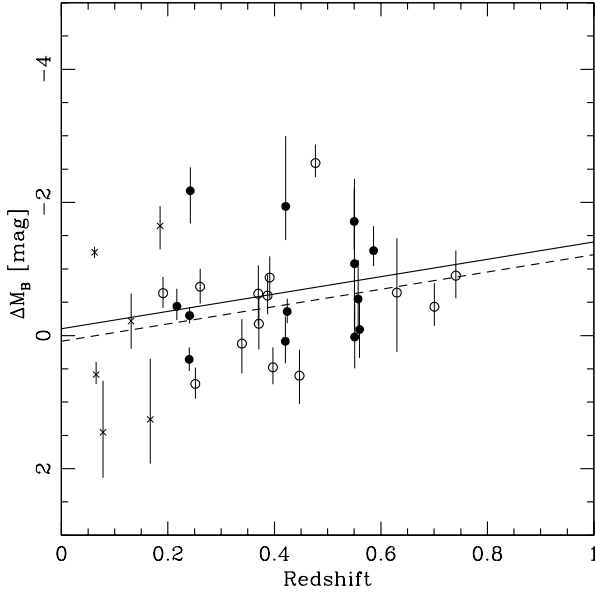


Figure 6. The TFR residuals from the local relation of PT92 as function of redshift. The symbols are the same as in Fig. 5. The dashed line shows a linear fit to the field galaxies at $z > 0.19$. The solid line is the same but for the cluster galaxies with the slope fixed to that of the field galaxies.

statistically-significant difference in the TFR between the cluster and field galaxies of our sample.

3.2 Rest-frame $B - V$ colours

We have seen that the TFR of the cluster galaxies in our sample looks similar to that of the field galaxies. In the previous section we found no evidence for a selection bias against star-burst galaxies introduced by our quality-control process. A further test for possible selection biases can be carried out if we look at the colour distributions of our samples, since galaxies with a strong star-formation episode would be very blue. Fig. 8 shows the rest-frame $B - V$ colour (Johnson-Morgan system) for all the galaxies in our sample with redshift and colour information available. The rest-frame colours were derived as described in Sec. 2.3. The results below do not change if we use observed colours which are independent of K-correction effects. In the figure, the cluster line-emission galaxies with rotation velocities unavailable (large triangles) do not show bluer colour compared with those with rotation velocities available (large circles). The mean rest-frame $B - V$ colour of these galaxies are 0.63 ± 0.05 and 0.61 ± 0.04 , respectively. Thus, the galaxies dropped in the rotation velocity measurement process are not significantly bluer than the ones we kept. Hence it is unlikely that we have statistically dropped cluster galaxies with higher star-formation from the rotation velocity measurement.

The possible existence of such bias for the field galaxies used in our TFR can be tested in the same way. The mean rest-frame $B - V$ colour of the field galaxies in the TFR is 0.55 ± 0.03 mag, while that of the field emission-line galaxies without secure rotation velocities is 0.57 ± 0.03 mag.

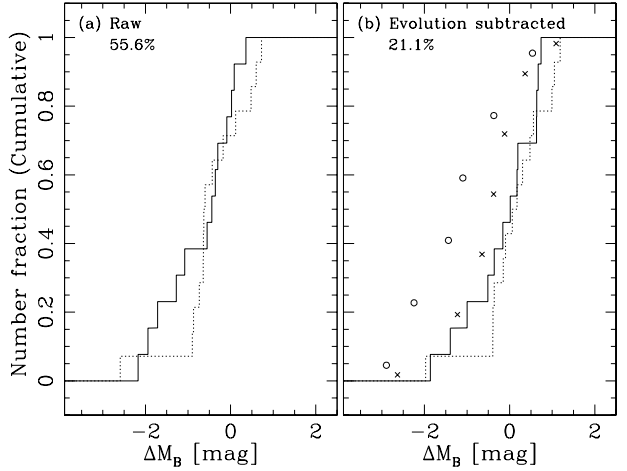


Figure 7. The cumulative distribution of the TFR residuals from the local relation of PT92 ($z > 0.19$ galaxies only). The solid and the dashed lines in panel (a) show the cluster and the field galaxies, respectively. The number at the left-top indicates the significance of the difference between the cluster and the field distributions from a Kolmogorov-Smirnov test. Panel (b) is the same as panel (a) but the measured luminosity evolution with redshift is subtracted using Eq. (1). The right panel also shows the cluster (circles) and field (crosses) galaxies from the 'matched' sample of B05A after subtracting the evolution in the same way (see text for details).

Thus the field galaxies used in the TFR sample well the field emission-line galaxies in terms of their colour distribution.

The colours allow us a further consistency check of our TFR result obtained in Sec. 3.1. Higher star-formation rates would produce bluer colours at the same time as excess B -band luminosity. The average rest-frame $B - V$ colour of the cluster galaxies used in the TFR is 0.61 ± 0.04 , while for the field galaxies it is 0.55 ± 0.03 . These values are only 1.2σ apart. If the cluster galaxies had higher star-formation than the field ones (as suggested by B05A), we would expect them to be bluer, and not redder. Furthermore, Fig. 9 shows no correlation between ΔM_B and $(B - V)_{\text{rest}}$ for either the field or the cluster galaxies. Such a correlation could be expected if excess star-formation were responsible for any excess luminosity in these galaxies. The distribution of the cluster and field galaxies in this diagram is indistinguishable. These two points are consistent with the fact that the TFR of the cluster galaxies in our sample is similar to that of the field galaxies.

As a final check, if we include all the emission galaxies in our colour test (i.e., not only those that make it into the TFR analysis) we still do not find any significant difference between the cluster and the field. The colour of all the emission galaxies in the clusters (0.62 ± 0.03) is slightly redder than that of field galaxies (0.56 ± 0.02), but the difference is again not significant. We will address quantitatively the colour and magnitude changes expected in different evolutionary scenarios in Sec. 5.1.

3.3 Spiral galaxies with absorption-line spectra

The presence of emission lines is a direct diagnostic for current star formation. The fraction of field spiral galaxies with

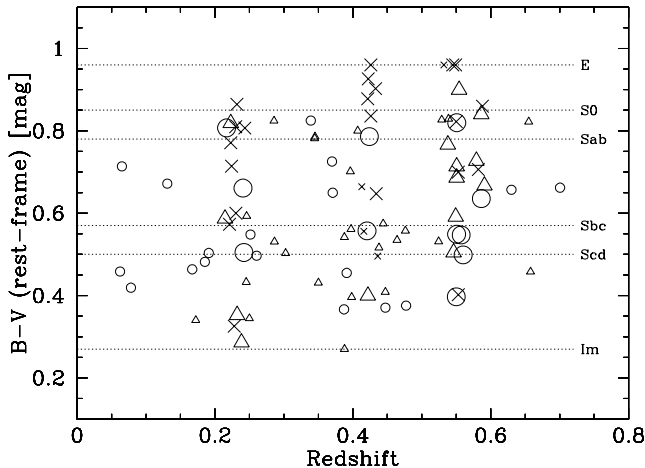


Figure 8. Rest-frame $B - V$ colour distribution of our sample galaxies. We plotted 93 of the 104 galaxies with known redshift, after dropping 9 galaxies with no colour information (see Sec. 2.3) and two galaxies at $z > 0.8$. The symbols are the same as Fig. 1. The dotted lines show the colours of E, S0, Sab, Sbc, Scd, and Im types at $z = 0$ from Fukugita et al.

no emission lines detected is $9 \pm 4\%$ (using Poissonian errors; see Table 2). For all the cluster galaxies (including suspected S0s), the fraction is much higher, $44 \pm 9\%$. Even if we exclude *all* the suspected S0 galaxies and the serendipitous elliptical (50% of the cluster galaxies with no emissions, Sec. 2.5), we estimate that in our sample at least $29 \pm 9\%$ of the spiral galaxies in the clusters have no emission lines. Thus, there is an excess of non star-forming spiral galaxies in the clusters compared with the field. Our data suggest a factor of at least ~ 3 difference, but it could be as high as a factor of ~ 5 . The existence of such ‘passive’ spiral galaxies in rich clusters is consistent with the results of Dressler et al. (1999): if (at least some) spirals transform into S0s when they fall into clusters, their star formation (and therefore their emission lines) must be switched off at some point. This result, coupled with the lack of difference found in the TFRs of the cluster and field spirals in our sample (Sec. 3.1), seems to suggest that the process leading to the eventual cessation of star-formation is not accompanied by a drastic star-burst event. This point will be explored further in Sec. 5.1.

The majority of the cluster absorption-line galaxies have colours typical of early-type galaxies, and the peak of their colour distribution is clearly different from that of emission-line galaxies. The mean rest-frame $B - V$ colour of the absorption-line galaxies in our clusters is 0.76 ± 0.04 , which is 0.20 ± 0.05 mag redder than the average colour of the field emission-line galaxies. A model star-burst containing 20% of the total stellar mass and solar metallicity reaches $(B - V)_{\text{rest}} \sim 0.7$ about 1 Gyr after the burst ended, and evolves very slowly thereafter ($(B - V)_{\text{rest}} \sim 0.8$ at ~ 2 Gyr; Bruzual & Charlot 2003). A truncated star-formation model behaves similarly. Thus the absorption-line galaxies in our sample have typically not experienced any significant star-formation for ~ 1 Gyr. However, there are a few absorption-line galaxies in our clusters that show bluer colours and are thus expected to be younger. This indicates that the sam-

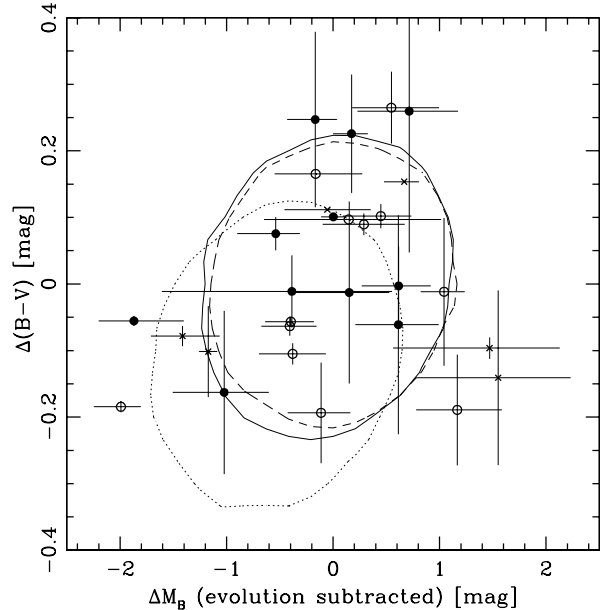


Figure 9. The TFR residuals vs. rest-frame $B - V$ colours for the 33 galaxies with secure rotation velocities. The redshift evolution has been subtracted using Eq. (1). The zero-point of the colours is set to the mean of the field galaxies. The symbols are the same as Fig. 5. The solid and dotted lines show the results of the simulation discussed in Sec. 5.1, indicating the regions where 68% of the cluster emission-line galaxies are distributed in models 9 and 1 respectively (see text for details). The dashed line is the same but for the field galaxies.

ple of absorption-line disk galaxies in our clusters contains galaxies at different stages in their evolution.

If we limit the above analysis to those galaxies with bona-fide spiral morphologies as determined from the HST images, the mean $B - V$ colour of the absorption-line galaxies in our clusters becomes 0.58 ± 0.10 . This is closer to the field emission-line galaxies, and would suggest a time sequence for the morphological transformation from spirals to S0s: spirals first switch off their star formation (i.e., no emission lines), and then become redder as their stellar populations age and their morphologies are transformed.

4 COMPARISON WITH PREVIOUS WORK

4.1 Detailed comparison

Before we can consider the implications of our results it is important to assess how reliable the rotation velocity measurements of intermediate redshift galaxies are. To carry out an external check, we compare our results with those of other work which uses a similar technique at comparable redshifts. We first compare the TFR of our field galaxies with the ones derived by other workers in Fig. 10. We plot the TFR residual vs. redshift to separate redshift evolution from other effects. We do not compare our results with studies which use emission line widths (e.g., Rix et al. 1997) instead of resolved rotation curves because that method is substantially different from ours, potentially causing significant systematic differences.

Vogt et al. (1996, 1997) investigated the TFR of 16 field galaxies at $0.15 \lesssim z \lesssim 1$ selected based on I -band magnitudes from Forbes et al. (1996), the Deep Extragalactic Evolutionary Probe project (Mould 1993), and the Hubble Deep Field (Williams et al. 1996). Eleven of the rotation curves obtained were labeled ‘high quality’ by them. The observed position-velocity diagrams were published for all the galaxies of their sample, and our visual inspection criteria also class these 11 as good-quality rotation curves. A visible turn-over point in the rotation curve was one of their quality-control criteria, as it is for us. Their results are consistent with the ones we found for our field galaxies.

Simard & Pritchett (1998) studied 12 field galaxies with $0.26 \leq z \leq 0.43$. The sample was selected by its strong [O II] emission (equivalent widths $> 20 \text{ \AA}$). The B -band absolute magnitude range of their sample was similar to that of Vogt et al. (1997). The measured rotation velocities were not corrected for inclination, so we applied an average correction to their galaxies before placing them on Fig. 10 by assuming $\langle V_{\text{obs}} \rangle = 0.7854 \langle V_{\text{edge-on}} \rangle$, which holds when galaxies are randomly oriented (cf. Simard & Pritchett 1998). We also remove two galaxies for which the derived error is larger than the derived rotation velocity. Since these authors did not publish the observed position-velocity diagrams, we could not compare our visual quality-control with theirs. We do not know whether a visible turn-over point of the rotation curves was one of their quality-control conditions. The TFR residuals of their sample are, on average, slightly brighter than in our field sample, although their redshift range and their sample size are small.

Ziegler et al. (2003) investigated the TFR of 13 cluster and 7 field galaxies with $0.3 \leq z \leq 0.6$ in three cluster fields. All the observed position-velocity diagrams were shown in Jäger et al. (2004), and 16 out of their 20 rotation curves pass our quality-control criteria, while four are rejected as rotation velocity overestimates. These authors also required a visible turn-over point in the rotation curves as one of their acceptance criteria. The TFR residuals of their field galaxies are consistent with the local galaxies of PT92, even at intermediate redshifts. Therefore, their field galaxies are slightly fainter than ours at a given rotation velocity, although their sample size is small.

Böhm et al. (2004) investigated the TFR of 77 field galaxies with redshifts between 0.1 and 1 in the FORS Deep Field. This work includes the galaxies studied by Ziegler et al. (2002). The sample was selected in the R band, requiring that the spectral energy distribution of the galaxies was later than E/S0. They selected 36 of their 77 galaxies as high quality, and for 18 of them the observed position-velocity diagram was shown. We agree with their quality assessment for these 18 galaxies, which are probably their best. A visible turn-over point of the rotation curve was one of their conditions for high quality, while those galaxies with a smaller extent or asymmetries were classified as low quality. The TFR residuals of their sample is consistent with that of our field sample. Naturally, our Eq. (1) agrees well with their resulting fit [see their Eq. (11)].

B05B, using the same sample as B05A (which includes also the data published by Milvang-Jensen et al. 2003), studied the properties of field spirals at intermediate redshift. Their sample contains 89 field galaxies with $0.1 \lesssim z \lesssim 1$. The observed position-velocity diagrams of six galaxies were

shown as an example in B05A, and our quality-control accepts five of them, while one is rejected as an underestimate. The main difference in the quality-control process of B05A with ours is that they placed less weight on the condition of a visible turn-over point, because ELFIT2PY should take that into account when estimating the errors (see B05A for details). For reference, we rejected 57% of the galaxies in our sample during the quality control process, while B05A rejected 47% of theirs. The TFR residuals from B05B are, at all redshifts, about 0.5 mag brighter than those from our sample, while the rate of redshift evolution (i.e., the slope in Eq. 1) is consistent. On panel (b) of Fig. 7 we compare the distribution of the TFR residuals from our Subaru sample with the ‘matched’ sample of B05A after removing the redshift evolution in the same way. A Kolmogorov-Smirnov test indicates that the distributions for field galaxies from both samples disagree with 98% confidence.

To finalise our comparison with previous work, we consider TFR studies that compare cluster and field galaxies. Ziegler et al. (2003) found no difference in the TFR between cluster and field galaxies, consistent with our result. We note that the behaviour of both the field and cluster galaxies of Ziegler et al. (2003) in the TFR residuals vs. redshift diagram is rather similar to that of ours. On the other hand, B05A (including Milvang-Jensen 2003 data), found that the average rest-frame B -band luminosity of cluster spirals was significantly ($\sim 0.7 \text{ mag}$) brighter than that of field ones at the same rotation velocity. We do not find that effect in our Subaru data. Panel (b) of Fig. 7 shows a comparison of our sample with that of B05A.

4.2 More on quality control issues

The visual quality control process is, perforce, subjective. The main difference found with some of the previous studies discussed above is the treatment of the turn-over point of the rotation curve. We find reasonable consistency between our results and those from studies that took the visible presence of a turn-over point in the observed velocity-position diagram as a requirement. It is therefore reasonable to expect that differences between our results and those from other studies (e.g., B05A) could be due to this issue.

Requiring a visible turn-over point has both advantages and disadvantages from a scientific point of view. If we require it, we may drop from our sample a number of small galaxies which undergo strong star formation (cf. ‘downsizing’ scenario), or cluster galaxies which may have more concentrated star-formation due to interactions with the cluster environment (cf. Moss & Whittle 2000). On the other hand, if we estimate the rotation velocity of a galaxy using a region that is too small (without reaching the turn-over point), the dark matter may not yet dominate, thus underestimating it. (e.g., Verheijen 2001). ELFIT2PY is designed to overcome this problem by direct 2-dimensional model spectrum fitting. So far, however, the possible systematics introduced by the software when no visible turn-over point is visible have not been explored. This is the main reason why, in this paper, we decided to use the visibility of the turn-over point as one of our quality-control conditions.

Detailed model simulations to test the behaviour of ELFIT2PY under different conditions are being carried out, and will be discussed elsewhere (Bamford et al. in prepara-

tion). Nevertheless, we have found that galaxies with small fitted emission-line scale-length tend to have brighter TFR residuals. Fig. 11(a) shows the Subaru TFR residuals as a function of the ratio between the fitted emission-line scale-length and the photometric disk scale-length. We show both the galaxies with secure rotation velocity determinations *and* those with insecure ones (i.e., the ones that did not pass our quality-control). The photometric disk scale-length is derived using GIM2D on the redest HST images, when available, and pre-imaging otherwise. If we look at all the emission-line galaxies in the figure, there is a trend in the sense that objects with smaller emission scale-lengths have brighter offsets in the TFR residuals. A possible explanation for this trend is that ELFIT2PY may tend to underestimate the rotation velocity for galaxies with smaller emission scale-lengths, but it could well be that these differences are real. On the other hand, the galaxies with *secure* rotation velocities (i.e., the ones used in the analysis) do not show such a trend, so this gives us some confidence in our quality-control/rejection process. Nevertheless, if concentrated emission is linked with increased star formation (and thus brightening), eliminating galaxies with compact emission from our analysis could hide some interesting and important physical effects. It is clear that using the presence or absence of a turn-over point in the rotation curve as a quality-control criterion is not as clear cut as one could naively expect, and it could significantly affect the conclusions.

In our sample, a significant fraction of the galaxies with a fitted emission scale-length smaller than the photometric disk scale-length tend to have insecure rotation velocity measurements. Many of them were rejected because they clearly underestimated the rotation velocity and/or have strong nuclear emission (cf. §2.4). It could be argued that an acceptance threshold should be introduced in the emission-line scale-length. A reasonable threshold could be set by $0.8 \times \langle \text{photometric disk scale-length} \rangle$ if our quality-control can be taken as optimal (cf. Fig. 11a). However, we decided not to impose such a strict limit and to use visual inspection to reject/accept measurements because we may lose some galaxies whose rotation velocities can be determined reasonably well but which have more centrally-concentrated star formation. These galaxies could provide important clues of the evolutionary processes taking place in the cluster environment (Moss & Whittle 2000; Milvang-Jensen 2003). This issue will be discussed in a future paper.

Fig. 11(b) shows an apparent correlation between the TFR residuals and the rotation velocity. We note that this correlation would be the natural consequence of the TFR residuals being a function of the rotation velocity [$\Delta M_B = 7.48 \log V_{rot} + \dots$]. The arrow on the panel shows the direction of the correlated errors. Although Böhm et al. claimed the same trend at $\log V_{rot} > 1.8$ as evidence of mass-dependent evolution (using a bootstrap bisector fit), the trend can also be explained by random errors in the rotation velocities for a magnitude-limited sample without requiring any evolution (see B05B). The insecure rotation velocity measurements tend to occupy the lower velocity region of this trend. This may be an indication that the rotation velocities of these galaxies could be systematically underestimated, although it is not possible to rule out that a real effect is present.

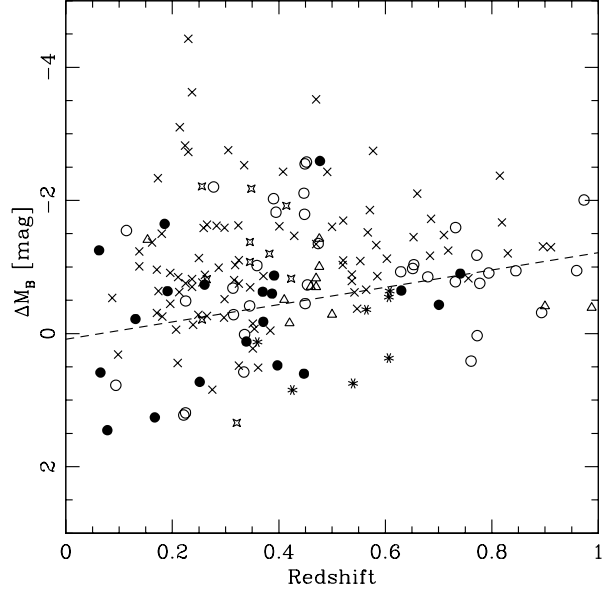


Figure 10. The TFR residuals of our field galaxies vs. redshift compared with those obtained from other studies. The cosmology and the face-on B -band extinction corrections are adjusted to match the ones adopted in this paper. The different symbols indicate: field galaxies in our sample (filled circles); high-quality galaxies from Vogt et al. (1996, 1997) (triangles); Simard & Pritchett (1998) (open stars); field galaxies from Ziegler et al. (2003) (asterisks); high-quality galaxies of Böhm et al. (2004) (open circles); and field galaxies from B05B (crosses). The dashed line is the same as in Fig. 6.

To summarise the above discussion, the subjectivity of the quality-control process, especially the treatment of the turn-over point of the rotation curve, can significantly change the TFR results, and it could be the source of discrepancies between different studies. It is thus important to present the data, including the observed position-velocity diagrams, in such a way that cross-checks between different samples and studies can be carried out. Of course, we must not forget other possible sources of discrepant results such as different instrument/telescope combinations or real physical differences between samples.

The discussion here illustrates the difficulties in comparing datasets observed by different groups and/or using different instruments. Even with the utmost care, inconsistencies are often unavoidable. But even if we cannot compare the galaxies in our Subaru sample with the ones in the VLT sample of B05A, the differences between field and cluster galaxies within each dataset should be more reliable because their field and cluster samples were selected, observed and analysed in exactly the same way. Since we cannot rule out that the differences between cluster and field galaxies found by B05A may be real, at this stage we will take their results at face value, as a working hypothesis, and explore the implications.

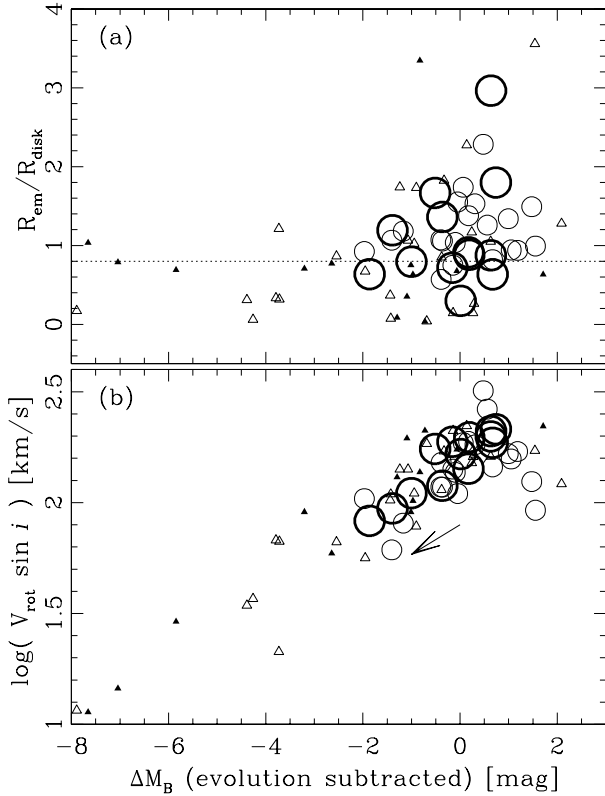


Figure 11. Panel (a): the TFR residuals as a function of the ratio between the fitted emission-line scale-length (R_{em}) and the photometric disk scale-length (R_{disk}) for all the galaxies with detected emission lines in the Subaru sample. The redshift evolution was subtracted using Eq. (1). Thick large and thin small circles denote the cluster and field galaxies with secure rotation velocities, respectively. The solid and open triangles represent the cluster and field galaxies with unreliable (i.e., rejected) measurements. The dotted line indicates where $R_{\text{em}} = 0.8 \times R_{\text{disk}}$. Below this line most measurements have been rejected (triangles). Panel (b): the TFR residuals as function of rotation velocity. The correction for inclination in the velocity is taken off to see the raw measured values. The arrow shows how an error in the rotation velocity changes the position of galaxies in this diagram. The direction and the dimension of the arrow corresponds to a 36% underestimate in the rotation velocity at a fixed magnitude, which results in making the TFR residuals 1 mag brighter.

5 IMPLICATIONS OF OUR RESULTS

We have seen no obvious difference between the cluster and the field emission galaxies in the TFR. This result is consistent with the results of Ziegler et al. (2003). We have also found no difference in the rest-frame $B - V$ colour distributions of the field and cluster emission-line spirals. On the other hand, we have detected a difference in the fraction of absorption-line spirals in our field and cluster samples. This is rather a puzzling situation, since this last result is usually interpreted as evidence for a transformation of spiral galaxies into S0s in cluster environments, while the first two results seem to suggest no difference in the cluster and field emission-line spirals. It is not impossible that, for a spiral galaxy sample like the one we have studied, the statisti-

cal effect on the colours and luminosities produced by the galaxy transformations we have postulated is too weak to be detected. This issue can only be addressed with detailed modeling.

The situation seems even more complicated if we accept the results of the study published by B05A, who found that cluster spirals are brighter than the field ones at the same rotation velocity, suggestive of a period of enhanced star-formation before it is switched off. Why don't we detect the same phenomenon? One possibility is that cluster-to-cluster differences could play an important role, although both studies concentrate on relatively rich clusters. Another possibility is that, due to the small number statistics, our Subaru sample may have missed several cluster galaxies that are undergoing this putative starburst, preventing us from detecting the same effect found by B05A. The likelihood of such possibility needs to be investigated.

To explore these two issues, we have computed several simulations of the expected changes in the statistical properties of field and cluster galaxy samples under different plausible evolutionary scenarios.

5.1 Model expectations

The basic assumption of our models is that field spiral galaxies fall into clusters and get transformed into S0s after their star formation is extinguished by the cluster environment (e.g., after their gas is removed by ram-pressure stripping). We start by assuming that the parent field galaxy is forming stars at a relatively constant rate. The star-formation history of such galaxy after it enters the cluster will depend on the details of its interaction with the intra-cluster medium, the cluster tidal field, other galaxies, etc. One possibility is a complete and sudden truncation of the star formation, as expected if *all* the gas is removed from the disk and halo of the galaxy. A second possibility is that the star formation ceases gradually (e.g., exponential decay), as expected if only the halo gas is removed while the gas disk is retained. In this case, the star formation will decay as the available gas is used up and not replenished from the halo reservoir. A third possibility is that in the interaction process, the halo gas is removed, and the disk gas is compressed, producing a period of enhanced star-formation leading to a rapid exhaustion of the gas reservoir. Our models explore these possibilities, and predict the observational consequences we would expect in a study like ours.

For the field galaxies we assume stellar populations with constant star formation and a fixed age of 5 Gyr. The results are not sensitive to this value provided that is larger than a few Gyrs. For the cluster galaxies we use the same model until the galaxy encounters the cluster. At that time, different star formation histories are considered, with different star-burst contributions and timescales. Fig. 12 shows some examples of the star-formation histories we used. The star formation after the encounter with the cluster has an e -folding timescale τ , with burst mass fraction f_b relative to the underlying population. Our calculations assume solar metallicity for the stellar populations, and use Bruzual & Charlot's (2003) models with a Chabrier (2003) initial mass function and the Padova 1994 stellar evolutionary tracks. Table 5 lists the values of the adopted model parameters (see below).

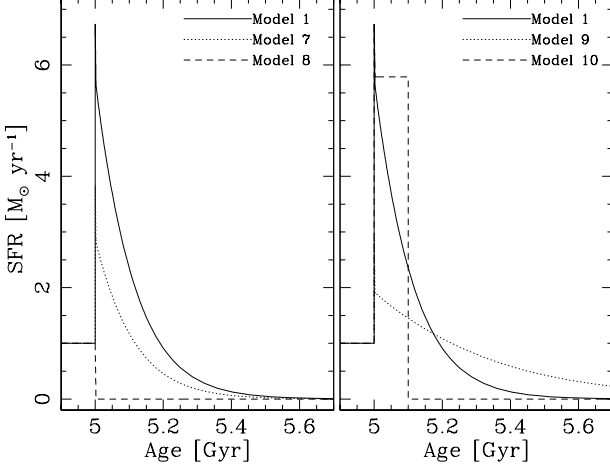


Figure 12. Examples of star-formation histories explored in our simulations. Model IDs correspond to those in Table 5. The absolute scale of the vertical axis is arbitrary.

We further assume that the parent field galaxies have a rest-frame B -band luminosity function like that determined from the 2dF survey by Norberg et al. (2002) for the local universe ($\alpha = -1.21$ and $M_B^* = -20.43$ with $h = 0.7$), and make M_B^* evolve with redshift according to Eq.(1), while keeping α constant. We select galaxies randomly from this luminosity function to generate a field population and a cluster population whose star-formation histories come from the models described above. We assume magnitude uncertainties of 0.1 mag, similar to the ones in our data. The magnitude limit of the model samples is set by the observed R -band magnitudes to mimic our observational selection. At each redshift, this R -band limit is translated into a value of $M_B(z)$ using our adopted cosmology and assuming the spectral energy distribution of the field galaxy models. Because of the way our observed samples were selected, this limit is reasonably close to M_B^* for the ‘quiescent’ field population. Obviously, we take into account that the star-formation history of a galaxy alters its luminosity and colours, bringing in or out of our simulated sample depending on its apparent magnitude.

We also assume that the field spirals retain their spiral morphology and emission line spectrum during the whole period covered by our simulations (i.e., they continue forming stars at a constant rate). This assumption seems reasonable for our sample since 91% of our field galaxies have detected emission lines (cf. Sec. 3.3). In the case of the cluster galaxies, we assume that the spiral morphology is observable for a time Δt_{sp} after their entrance in the cluster/start of the possible burst. After that time, the cluster galaxies do not enter our sample since they would not be classified as spirals anymore. That defines the maximum age of the cluster galaxies in our simulated samples. It is important to remember that the absorption-line galaxies in our cluster sample could be contaminated by S0s when considering the results of our simulations.

Thus, a population of infalling cluster spirals is built in our simulations by randomly-sampling the field luminosity function and assigning to the galaxies an age t_b counted from their entrance in the cluster/start of the burst. This

age is taken randomly from the interval ($0 \leq t_b \leq \Delta t_{sp}$). The corresponding magnitude change in each band is determined from the model. Obviously, if t_b is comparable to or smaller than τ , the galaxy would be brighter than the parent galaxy because of the starburst. At later times, it would become fainter due to the cessation of star formation and the aging of the stellar population. The magnitude limit determines whether the galaxy enters the sample or not. If the galaxy ends up in the sample, a rotation velocity is assigned to it using the TFR of PT92 assuming luminosity evolution from Eq.(1). In this process the luminosity that we use to determine the galaxy’s rotation velocity is the one it had *before* it entered the cluster. The underlying assumption is that the interaction with the cluster environment alters the galaxies’ luminosities (via a change of their star formation histories), but not their masses/rotation velocities. The error in $\log V_{rot}$ (km s^{-1}) is set to 0.1, comparable with our data. A comparison sample of field spiral galaxies is built by randomly populating the field luminosity function down to our apparent magnitude limits, and assigning rotation velocities to them in a similar way.

We further define the parameter Δt_{em} ($0 \leq \Delta t_{em} \leq \Delta t_{sp}$) by requiring that emission lines are observables only if $t_b \leq \Delta t_{em}$. This parameter controls the fraction of absorption-line spiral galaxies. Note that this is not a free parameter since the equivalent width (EW) of the emission lines (and therefore their detectability) depends on the relative intensity of the star formation at any given time, and therefore it is possible to estimate reasonable values of Δt_{em} for each model (see below).

The observed redshift z_{obs} is set to 0.4, which is close to the median of our sample (Sec. 2.2). We set $\Delta t_{sp} = 3$ Gyr, based on the numerical simulations of gas stripping by Bekki, Couch, & Shioya (2002), and $\tau = 0.1$ Gyr following Quilis et al. (2000). For each model, Δt_{em} is determined by considering reasonable observational limits in the EW of the emission lines. The number of ionising (Lyman continuum) photons, N_{Ly} , is taken from the population synthesis models, and used to calculate the $H\alpha$ luminosity as $L(H\alpha) = 1.36 \times 10^{-12} \cdot N_{Ly}$ (erg s^{-1}). Our calculations assume that all the ionising photons from the hot stars are absorbed (case B recombination), an electron temperature $T_e = 10^4$ K and an electron density $n_e = 100 \text{ cm}^{-3}$. We further apply a mean extinction of $A_V = 1.1$ mag to the emission lines, as derived for nearby SDSS spirals by Nakamura et al. (2004). Seaton (1979) extinction law is then used to derive the EW of the line from the line and continuum luminosities of the models. The observational threshold is set to 10\AA for $H\alpha$, which is more or less similar to that of our observations. Note that because the extremely rapid evolution of the EW after the star-formation has ceased (see, e.g., Alonso-Herrero et al. 1996), a factor two difference in the EW limit does not affect Δt_{em} significantly. Equally, setting the limit using a different line would make very little different. For the burst strength f_b we use a reasonably high value of 0.2 initially. The model calculated with this set of parameters is called our ‘standard’ model (number 1). We will explore later the effect of varying these parameters (cf. Table 5), and the star formation histories (see Fig. 12).

We simulate cluster and field galaxy samples containing 1000 galaxies each. The results of the simulations in terms of observable quantities are summarized in Table 5. The mod-

els achieving relatively close values to the observed ones are marked with stars. The values of the scatter shown in the table represent the standard deviations for the simulated galaxy samples², and the observational errors for the observed quantities. The standard deviations of the predicted quantities for the simulated field galaxies depend only on the assumed errors. As the table caption indicates, the standard deviation of ΔM_B for the simulated field galaxies at $z = 0.4$ is 0.77, remarkably close to that of our observed field TFR (0.78; see Sec. 3.1). For the cluster galaxies, the scatter also depends on both the brightening of galaxies due to the burst of star formation and the fading of galaxies in the fade-out phase after the event. Nevertheless, assuming errors comparable to those of our observations, we find that the scatter in the observed properties of field and cluster galaxies are almost the same, and consistent with the observed ones. Since we are interested in relative differences between the cluster and the field galaxies, we ignore possible offsets between the absolute colours of the models and the observed galaxies. For simplicity, we also ignore the fact that actual spiral galaxies show a wider spread in colour than our models due to differences in morphology, inclination, extinction, stellar populations, metallicities, etc. We expect differential quantities to be more robust than absolute ones.

As a first step, we explored the effects of varying some of the parameters on the predicted differences between the cluster and field model galaxies. We found that the dependence of the model results on the actual value of z_{obs} is small (see Models 2 and 3). This is due to the fact that our observations were designed to reach approximately the same absolute magnitude at each redshift. Thus using our fiducial value $z_{obs} = 0.4$ to model our complete dataset should be safe. The value of Δt_{sp} that best corresponds to our Subaru sample is not well defined by our galaxy selection procedure. Luckily, changing this parameter within very broad limits has almost negligible effect on the predicted differences between field and cluster model galaxies (Models 4 and 5). Changing the magnitude limit of the observations has only a moderate effect (Model 6): going deeper in the luminosity function changes the results a little by including a few more galaxies in the fade-out phase in the galaxy samples.

The main conclusion of exploring models 1–6 is that with the parameters explored there we do not get results which simultaneously agree with our observed changes in luminosity, colour and absorption-line galaxy fraction. A better match to our observations is achieved if we reduce the burst strength f_b to 0.1 (Model 7). A truncated star formation history without a star-burst (Model 8) also predicts close values to our observations in terms of magnitude and colour differences because cluster emission-line galaxies spend a very short time in the emission phase, and thus do not have time to make their properties different from the field galaxies. However, the fraction of absorption-line galaxies ends up being too high for this model since the vast majority of the cluster galaxies would have stopped forming stars. Alternatively, our observed values are roughly

achieved also if the burst timescale is as long as ~ 0.3 Gyr (Model 9).

The magnitude and colour distributions from Models 1 and 9 are over-plotted in Fig. 9. It seems as if Model 9 not only provides a better match to the average observed values, but also to their distributions. However, our models tell us that there is a degeneracy between the burst mass fraction and the star-formation time scale. Models 7 and 9 reproduce the observations almost equally well. Nevertheless one interesting conclusion is that it is possible to have substantial starbursts in the cluster spirals without significantly changing the average colours and luminosities of the population of line-emitting spiral galaxies in a sample like ours. It is also clear that the scenario we propose would imply a significant increase in the fraction of spiral galaxies with absorption-line spectra when the field galaxies fall into the clusters, as observed.

On the other hand, B05A found that the mean TFR residuals of the cluster galaxies are 0.7 mag brighter than that of the field galaxies, in agreement with the earlier findings of Milvang-Jensen et al. (2003). This is closer to the predictions of more massive or shorter timescale bursts (e.g., Model 1) than our case. If we assume that the results from B05A can be represented by Model 1, the difference from the Subaru observations would be $\sim 1.1\sigma$ in terms of $\Delta_f^{c,em}(\Delta M_B)$ ($\sim 1.6\sigma$ when compared with B05A directly as opposed to comparing with the model). However, the difference would be $\sim 4.5\sigma$ in terms of $\Delta_f^{c,em}(B - V)$, i.e., the model predicts significantly bluer cluster emission-line galaxies. Taken at face value, this implies a very low probability that the discrepancies in the results from the VLT and Subaru data are due simply to a different sampling of the same parent population. Of course, this assumes that one can apply simple Gaussian statistics to this complex problem, which is far from clear.

Thus, we cannot rule out that other factors not accounted for in our simulation could also play some role in the observed differences. The lower median redshift of the Subaru sample (0.39), as compared with the VLT one (0.52), would suggest that one would expect a stronger evolutionary effect for the latter. However, B05A show that the effect is present for even their lower redshift clusters ($z \sim 0.3$). Cluster-to-cluster differences are, of course, another potential candidate.

The fact that we get a relatively weak statistical significance for the inconsistency between the Subaru results and Model 1, or between the Subaru data and the VLT data of B05A in terms of $\Delta_f^{c,em}(\Delta M_B)$ is due to the large uncertainties associated with the measured values. Indeed, according to our model simulations, one would need to determine reliable rotation velocities for ~ 50 cluster spirals and a similar number of field ones to distinguish Model 1 (strong, short burst) from Model 9 (weak burst with slowly-declining star formation) at 3σ level by using $\Delta_f^{c,em}(\Delta M_B)$ alone. Thus much larger samples than those presented here and in B05A are needed.

5.2 Evolution of star formation rate with redshift

The evolution of the B -band absolute magnitude with redshift for the field spirals in our sample (Eq. (1) and Fig. 6) can be interpreted as due to the evolution of the star-

² The error in the mean values can thus be obtained by dividing the standard deviation by $(N - 1)^{1/2}$, where $N = 1000$ is the number of galaxies in the simulations.

Table 5. Model predictions for different parameters: The values of the model parameters for the standard model are discussed in the text. Only the parameters that change in each model are listed. The remaining parameters are as in the standard model. The models achieving values close to the observed ones are marked with stars.

Model # and Item	Δt_{em} (Gyr)	$\Delta_f^{c,em}(\Delta M_B)^a$ (mag)	$\Delta_f^{c,em}(B-V)^b$ (mag)	$\Delta_f^{c,abs}(B-V)^c$ (mag)	$f_{c,abs}^d$ (%)
(1) Standard model $z_{obs} = 0.4$, $\Delta t_{sp} = 3$ Gyr, $M_{lim} = M_B^*(z)$, $f_b = 0.2$, $\tau = 0.1$ Gyr	0.26	-0.54 ± 0.82	-0.12 ± 0.15	0.16 ± 0.19	45
(2) $z_{obs} \rightarrow 0.2$	0.26	-0.52 ± 0.79	-0.10 ± 0.15	0.26 ± 0.22	53
(3) $z_{obs} \rightarrow 0.6^e$	0.26	-0.52 ± 0.81	-0.10 ± 0.15	0.15 ± 0.20	31
(4) $\Delta t_{sp} \rightarrow 1$ Gyr	0.26	-0.49 ± 0.75	-0.11 ± 0.14	0.14 ± 0.17	42
(5) $\Delta t_{sp} \rightarrow 8$ Gyr ^e	0.26	-0.54 ± 0.77	-0.11 ± 0.15	0.19 ± 0.21	46
(6) $M_{lim} \rightarrow M_B^*(z) + 2$ mag	0.26	-0.42 ± 0.83	-0.11 ± 0.15	0.33 ± 0.22	76
(7) $f_b \rightarrow 0.1$ *	0.22	-0.12 ± 0.77	-0.03 ± 0.16	0.23 ± 0.19	46
(8) $f_b \rightarrow 0.0^f$	0.002	0.10 ± 0.98	0.02 ± 0.19	0.25 ± 0.18	99
(9) $\tau \rightarrow 0.30$ Gyr *	0.57	-0.03 ± 0.76	0.00 ± 0.16	0.27 ± 0.17	30
(10) Burst type : Exp. \rightarrow Const.	0.11	-0.96 ± 0.76	-0.20 ± 0.15	0.13 ± 0.20	60
Observed ^g		-0.18 ± 0.33	0.06 ± 0.04	0.20 ± 0.05	20–34

^a Difference in TFR residuals between cluster and field galaxies, and the *standard deviation* for the *cluster* galaxies (see text). The average residual for the field galaxies and its standard deviation at $z = 0.4$ is $\Delta M_{B,f} = -0.50 \pm 0.77$.

^b Difference in rest-frame $B - V$ colour between the emission-line galaxies in the clusters and the field, and the standard deviation for the *cluster* galaxies. The average colour of the field galaxies and its standard deviation is $(B - V)_f = 0.34 \pm 0.14$.

^c The same as *b*, but for the absorption-line galaxies.

^d Fraction of absorption-line cluster galaxies. Note that the observed fraction shows the measured fraction of cluster absorption-line spirals minus the measured fraction of field absorption-line spirals. This is done because our models assume that all the field spirals have emission lines.

^e The nominal ages of the model for the cluster galaxies can exceed the age of the universe, although such galaxies are in the fade-out phase and thus insensitive to the assumed age of the underlying population at the time of the burst.

^f No starburst (truncated star-formation).

^g The observed mean values with 1σ errors except for $f_{c,abs}$, where we give the accepted range.

formation rate (SFR) of these galaxies. In this section, we parameterise the SFR evolution as a simple power law of the form $SFR \propto (1+z)^\alpha$, and estimate the value of α that best explains our result. In order to calculate the luminosity evolution in the B -band associated with the postulated SFR evolution we used Bruzual & Charlot (2003) models with a Chabrier (2003) initial mass function and solar metallicity. The results are shown in Fig. 13. Changing the formation epoch of the galaxies in the range $1 < z < 5$ hardly affects our estimated α for $\alpha \lesssim 2$. Thus, we arbitrarily set the time at which spirals start forming stars at 20% of the Universe’s present-day age ($z_f = 2.7$ with the adopted ‘concordance’ cosmology). Note that if the SFR had remained constant with time ($\alpha = 0$), spiral galaxies would get slightly fainter with redshift in the B band as the building up of their stellar populations with time slightly overcompensates the average ageing of their stellar populations. Since our observations indicate that spiral galaxies get brighter with redshift, their SFR must be higher at higher z , i.e., $\alpha > 0$.

To compare our observational results with the model predictions, and to increase the statistic accuracy, we compute the weighted-mean of the slopes in Eq. (1) and in B05B (-1.0 ± 0.5), and interpret it as the representative of the evolution of field spiral galaxies at the median redshift of the VLT and Subary field galaxy samples. We obtain $\Delta M_B = -0.51 \pm 0.22$ mag at $z = 0.48$, which is shown in Fig. 13 as the data-point with errorbars. Taken at face value, our analysis yields $\alpha = 1.7 \pm 0.7$.

This value could be an overestimate of the rate of evolution for two reasons. First, in our analysis we have assumed constant (solar) metallicity for the spiral galaxies. It is reasonable to expect that the average metallicity of field spirals might have been lower in the past, and, for a given stellar mass, a lower metallicity stellar population is expected to be brighter in B (see, e.g., Bruzual & Charlot 2003). Thus, part of the observed luminosity evolution may be caused by a change in the average metallicity of the stellar populations of the galaxies. However, we expect this effect to be

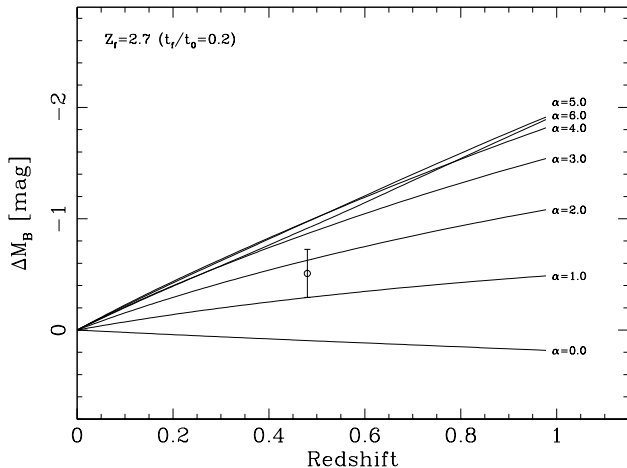


Figure 13. The evolution of B -band absolute magnitude with redshift for galaxies with different star-formation histories. The lines show the model predictions with $SFR \propto (1+z)^\alpha$ for different values of α and solar metallicity. The circle with the errorbar shows the slope derived from Eq. (1) combined with the one derived by B05B placed at the median redshift of the combined field TFR sample.

small because the measured evolution in the average metallicity of field galaxies is rather modest (cf. Kobulnicky et al. 2003; Lilly, Carollo & Stockton 2003; Kobulnicky & Kewley 2004). At the median redshift of our field galaxy sample we expect the average metallicity (at a given galaxy mass) to be only ~ 0.07 dex lower than at $z = 0$ (Kobulnicky & Kewley 2004), which would have negligible effect in our calculation. The second reason why we may have overestimated the rate of SFR evolution is that any unaccounted for selection effects probably mean that we preferentially select intrinsically brighter galaxies at high- z , thus increasing the apparent luminosity evolution.

This rate of SFR evolution is substantially shallower than the rate of evolution of the SFR density of the universe indicated by studies based on the UV, H α , far-infrared, and radio emission of galaxies, which all suggest $\alpha \sim 3$ –4 between $z = 0$ and 1 (e.g., Hopkins 2004). Hence, the rapid evolution in the cosmic SFR density is not driven by the evolution in the SFR of individual bright ($M_B \lesssim M_B^*$) spiral galaxies like the ones in our sample, in agreement with the conclusions of B05B.

6 SUMMARY

We have carried out MOS observation of 4 cluster fields using the FOCAS spectrograph at Subaru, and obtained spectra of 103 cluster and field spiral galaxies with spectroscopic redshifts in the range $0.06 \leq z \leq 1.20$. A total of 77 galaxies show emission lines. Of these, 33 galaxies yielded observed rotation curves of good enough quality to determine secure rotation velocities. Our sample reaches roughly M_B^* at each redshift.

By comparing the rest-frame B -band Tully-Fisher relation (TFR) of our cluster and field emission-line spiral galaxies, we found no measurable difference between the B -band luminosity at a given rotation velocity of both populations.

This agrees with the conclusions of Ziegler et al. (2003), but disagrees with our own previous VLT results (Milvang-Jensen et al., 2003; Bamford et al. 2005A). We also find the rest-frame $B - V$ colour of the cluster emission-line galaxies is marginally redder (by 0.06 ± 0.04) than that of the field galaxies, providing little indication that the cluster spirals are undergoing enhanced star formation. On the other hand, we find that the fraction of spiral galaxies with absorption-line spectra (i.e., no detectable emission lines) in the clusters is larger than that in the field by a factor ~ 3 –5, in agreement with the results of Dressler et al. (1999). This implies that the cluster environment quenches star-formation on its spiral galaxies, leading, perhaps, to the formation of S0s.

To evaluate the significance of our results, we carried out simulations of the effects that changes in the star-formation history of in-falling spiral galaxies would have on the observed properties of galaxy samples similar to ours. Following the encounter of the in-falling galaxies with the cluster environment, our models explore different star-formation scenarios, including truncation of the galaxies’ star-formation on different timescales, possibly preceded by bursts of different strengths. It turns out that even quite drastic changes in the SFR of the galaxies may have quite modest effect on the average luminosity and colour of a sample of bright cluster spiral galaxies *selected to have ongoing star-formation* (i.e., having the strong emission lines needed for rotation-curve measurement). However, the fraction of spiral galaxies with absorption-line spectra (i.e., without current star-formation) is very sensitive to the effect of star-formation truncation. Our Subaru observations favour models with relatively mild or absent initial star-bursts, and relatively long star-formation timescales, while the VLT results of Bamford et al. favour a more massive initial star-burst and a shorter time-scale. However, we estimate the probability that the observed difference between our Subaru results and the VLT ones of Bamford et al. arises from “unlucky” statistic sampling of galaxy populations with intrinsically similar properties. We find that both Tully-Fisher relation results are only different at the $\sim 1\sigma$ level. This is due to the relatively small sample sizes and the large uncertainties in the determination of the individual TFR offsets. To definitively rule out the presence of a starburst before the star-formation cessation would require samples of ~ 50 –100 field and cluster spirals with reasonable determinations of their rotation velocity.

Finally, we find that the rest-frame absolute B -band magnitude (at a fixed rotation velocity) of the field galaxies in our sample shows an evolution of -1.30 ± 1.04 mag per unit redshift. By statistically-combining our luminosity evolution estimate with that of Bamford et al. (2005B; -1.0 ± 0.5 mag per unit redshift), and interpreting it as due to the increase with redshift of the SFR of the galaxies, we estimate that $SFR \propto (1+z)^{1.7 \pm 0.7}$ for our field spirals. This indicates that the average SFR of bright ($M_B \lesssim M_B^*$) disk galaxies evolves more slowly than the universal SFR density, suggesting that the evolution of the global SFR evolution is not dominated by bright star-forming disk galaxies, in agreement with previous studies.

ACKNOWLEDGMENTS

We would like to thank Yoshihiko Yamada and Masato Onodera for preparation of the proposal for the observations. We also thank the referee, Asmus Böhm, for his very useful comments. The work is partly supported by a Grant-in-Aid for Scientific Research (No. 16540223) by the Japanese Ministry of Education, Culture, Sports, Science and Technology. This work is partly based on observations made with the NASA/ESA *Hubble Space Telescope*, obtained from the data archive at the Space Telescope Institute. STScI is operated by the association of Universities for Research in Astronomy, Inc. under the NASA contract NAS 5-26555.

REFERENCES

- Abadi M. G., Moore B., Bower R. G., 1999, MNRAS, 308, 947
- Alonso-Herrero, A., Aragón-Salamanca, A., Zamorano, J., Rego, M., 1996, MNRAS, 278, 417
- Balogh M. L., Schade D., Morris S. L., Yee H. K. C., Carlberg R. G., Ellingson E., 1998, ApJ, 504, L75
- Bamford S., Aragón-Salamanca A., Milvang-Jensen B., 2005, MNRAS, submitted [B05B]
- Bamford S., Milvang-Jensen B., Aragón-Salamanca A., Simard L., 2005, MNRAS, accepted [B05A]
- Bekki K., Couch W. J., Shioya Y., 2002, ApJ, 577, 651
- Bertin E., Arnouts S., 1996, A&AS, 117, 393
- Böhm A., et al., 2004, A&A, 420, 97
- Bruzual G., Charlot S., 2003, MNRAS, 344, 1000
- Chabrier G., 2003, PASP, 115, 763
- Couch W. J., Ellis R. S., Sharples R. M., Smail I., 1994, ApJ, 430, 121
- Couch W. J., Sharples R. M., 1987, MNRAS, 229, 423
- Dressler A., Gunn J. E., 1983, ApJ, 270, 7
- Dressler A., Gunn J. E., 1992, ApJS, 78, 1
- Dressler A., Smail I., Poggianti B. M., Butcher H., Couch W. J., Ellis R. S., Oemler A. J., 1999, ApJS, 122, 51
- Dressler A., et al., 1997, ApJ, 490, 577
- Ellingson E., Yee H. K. C., Abraham R. G., Morris S. L., Carlberg R. G., 1998, ApJS, 116, 247
- Ellingson E., Yee H. K. C., Abraham R. G., Morris S. L., Carlberg R. G., Smecker-Hane T. A., 1997, ApJS, 113, 1
- Fasano G., Poggianti B. M., Couch W. J., Bettoni D., Kjærgaard P., Moles M., 2000, ApJ, 542, 673
- Forbes D. A., Phillips A. C., Koo D. C., Illingworth G. D., 1996, ApJ, 462, 89
- Fukugita M., Shimasaku K., Ichikawa T., 1995, PASP, 107, 945
- Ghigna S., Moore B., Governato F., Lake G., Quinn T., Stadel J., 1998, MNRAS, 300, 146
- Hopkins A. M., 2004, ApJ, 615, 209
- Jäger K., Ziegler B. L., Böhm A., Heidt J., Möllenhoff C., Hopp U., Mendez R. H., Wagner S., 2004, A&A, 422, 907
- Jones L., Smail I., Couch W. J., 2000, ApJ, 528, 118
- Kashikawa N., et al., 2002, PASJ, 54, 819
- Kobulnicky, H.A., et al., 2003, ApJ, 599, 1006
- Kobulnicky, H.A., Kewley, L.J., 2004, ApJ, 617, 240
- Kodama T., Bower R. G., 2001, MNRAS, 321, 18
- Kodama T., Smail I., 2001, MNRAS, 326, 637
- Lilly, S.J., Carollo, C.M., Stockton, A.N., 2003, ApJ, 597, 730
- Mihos J. C., McGaugh S. S., de Blok W. J. G., 1997, ApJ, 477, L79
- Milvang-Jensen B., 2003, PhD Thesis, University of Nottingham
- Milvang-Jensen B., Aragón-Salamanca A., Hau G. K. T., Jørgensen I., Hjorth J., 2003, MNRAS, 339, L1
- Moore B., Katz N., Lake G., Dressler A., Oemler A., 1996, Natur, 379, 613
- Moss, C., Whittle, M., 2000, MNRAS, 317, 667
- Mould J., 1993, ASPC, 43, 281
- Mulchaey J. S., Zabludoff A. I., 1998, ApJ, 496, 73
- Nakamura O., Fukugita M., Brinkmann J., Schneider D. P., 2004, AJ, 127, 2511
- Norberg P., et al., 2002, MNRAS, 336, 907
- Persic M., Salucci P., 1991, ApJ, 368, 60
- Pierce M. J., 1994, ApJ, 430, 53
- Pierce M. J., Tully R. B., 1992, ApJ, 387, 47 [PT92]
- Poggianti B. M., Smail I., Dressler A., Couch W. J., Barger A. J., Butcher H., Ellis R. S., Oemler A. J., 1999, ApJ, 518, 576
- Quilis V., Moore B., Bower R., 2000, Sci, 288, 1617
- Rix H., Guhathakurta P., Colless M., Ing K., 1997, MNRAS, 285, 779
- Schlegel D. J., Finkbeiner D. P., Davis M., 1998, ApJ, 500, 525
- Schneider D. P., Gunn J. E., Hoessel J. G., 1983, ApJ, 264, 337
- Seaton M. J., 1979, MNRAS, 187, 73P
- Simard L., Pritchett C. J., 1998, ApJ, 505, 96
- Simard L., Pritchett C. J., 1999, PASP, 111, 453
- Simard L., et al., 2002, ApJS, 142, 1
- Thuan T. X., Gunn J. E., 1976, PASP, 88, 543
- Toomre A., Toomre J., 1972, ApJ, 178, 623
- Tully R. B., Fouque P., 1985, ApJS, 58, 67
- van Dokkum P. G., Franx M., Kelson D. D., Illingworth G. D., Fisher D., Fabricant D., 1998, ApJ, 500, 714
- Verheijen M. A. W., 2001, ApJ, 563, 694
- Vogt N. P., Haynes M. P., Giovanelli R., Herter T., 2004, AJ, 127, 3300
- Williams R. E., et al., 1996, AJ, 112, 1335
- Yee H. K. C., Ellingson E., Abraham R. G., Gravel P., Carlberg R. G., Smecker-Hane T. A., Schade D., Rigler M., 1996, ApJS, 102, 289
- Zabludoff A. I., Mulchaey J. S., 1998, ApJ, 496, 39
- Ziegler B. L., et al., 2002, ApJ, 564, L69
- Ziegler B. L., Böhm A., Jäger K., Heidt J., Möllenhoff C., 2003, ApJ, 598, L87